Research Square

Preprints are preliminary reports that have not undergone peer review.
They should not be considered conclusive, used to inform clinical practice,
or referenced by the media as validated information.

Rational design of bovine milk transferrin-derived peptides as allosteric modulators of FtsZ

Mustafa Hussein Hamad
Lorestan University
Vali Akbari
akbari.v@lu.ac.ir

Lorestan University
Armin Zarei
Kermanshah University of Medical Sciences

Article

Keywords: Bovine milk lactoferrin, FtsZ Inhibition, MD simulations, MM/PBSA, Peptide inhibitors

Posted Date: September 24th, 2026

DOI: https://doi.org/10.21203/rs.3.rs-10898516/v1

License: This work is licensed under a Creative Commons Attribution 4.0 International License.
Read Full License

Additional Declarations: No competing interests reported.

Rational design of bovine milk transferrin-derived peptides as allosteric modulators of FtsZ

Mustafa Hussein Hamad [a], Vali Akbari[*b], Armin Zarei[c]

[a] *MSc student, Department of Biology, Faculty of Basic Sciences, Lorestan University, Khorramabad, Iran.*

[b] *Department of Biology, Faculty of Basic Sciences, Lorestan University, Khorramabad, Iran.*
[c] *Pharmaceutical Sciences Research Center, Health Institute, Kermanshah University of Medical Sciences, Kermanshah, Iran*

Abstract

Fast and growing spread of antibiotic resistance demands new antibacterial strategies beyond conventional drug classes. The bacterial cell-division protein FtsZ, essential for cytokinesis via Z-ring assembly, offers a validated yet underexploited target, particularly its allosteric interdomain cleft recognized by the inhibitor PC190723. In this study, we are motivated by bovine milk lactoferrin—a pharmaceutical protein with well-documented antibacterial properties—as a novel template for designing novel peptides against FtsZ. Molecular docking between the template and the FtsZ PC-binding site recognized a 10-residue peptide template, which was refined through MM/PBSA-guided mutagenesis at three hotspot positions (65, 69, 70), producing a mutant peptide library subsequently screened for toxicity, allergenicity, and binding affinity against the target. Among the candidates, PEP44 and PEP58 emerged as top performers, achieving the strongest HADDOCK docking scores and the highest MM/PBSA binding energies (−243.13 and −230.10 kJ/mol, respectively), driven by complementary electrostatic and hydrophobic anchoring mechanisms. Molecular dynamics (MD) simulations confirm that both peptides preserve native FtsZ conformational dynamics while stabilizing the interdomain cleft, consistent with an allosteric inhibitory mode resembling PC190723. These findings establish, for the first time, a milk-protein-derived peptide design pipeline against FtsZ and nominate PEP44 and PEP58 as promising leads for experimental validation as next-generation antibacterial agents.

Keywords: Bovine milk lactoferrin, FtsZ Inhibition, MD simulations, MM/PBSA, Peptide inhibitors

[*] Corresponding author: *E-mail address:* akbari.v@lu.ac.ir (Vali Akbari)

1. Introduction

The escalation of resistance to several antibiotics among bacterial pathogens as well as limited improvement in the discovery of novel antimicrobial medications, highlights the urgent need for promising treatment methods [1]. One of the interesting option for developing alternative therapies is to identify novel molecular targets for antimicrobial drug design, a concept that has gained significant attention in recent years [2]. Traditionally, clinically used antibiotics induce their effects by interfering essential cellular activities, including protein production, RNA synthesis, DNA duplication, peptidoglycan generation in the cell wall, folate pathway metabolism, and the integrity or function of the cytoplasmic membrane [2,3]. Cell division in bacteria is an important procedure required for microbial pathogenicity and growth and, yet it has not been extensively used for clinical therapies. A key component that coordinates this process in most bacterial species is Filamentous temperature-sensitive mutant Z (FtsZ) [4]. This enzyme has arisen as a promising antibacterial target owing to its indispensable association with prokaryotic cytokinesis [4]. During bacterial proliferation, cellular division is coordinated by the divisome, a complex multiprotein machinery assembled at the midcell region [4]. Among its components, FtsZ functions as the primary organizer recruited to the prospective septation site, where it polymerizes into a dynamic Z-ring scaffold [4]. This structure not only directs the localization of additional division proteins, but also drives membrane invagination through constant polymer remodeling [4,5]. This bacterial enzyme is of promising potential as target to discover novel antibiotics, which lay down a couple of reasons: first of all, successful suppressing FtsZ enzymatic function can lead to ceasing the cell division to exist, and promote bacterial lysis [5]. Second of all, although FtsZ is highly conserved among bacterial species, it is absent in eukaryotic cells and exhibits limited sequence similarity to tubulin, thereby reducing the likelihood of off-target toxicity in humans [5,6].

Structurally speaking, FtsZ contains two ligand-binding pockets: the nucleotide-binding domain and the inter-domain cleft [7,8]. The nucleotide-binding pocket, located in the N-terminal subdomain (form residues 13 to 173) (**Fig. 1**), regulates GTP binding and hydrolysis, controlling protofilament assembly and bacterial cytokinesis [7,8]. Since this region is highly conserved across bacterial species, it represents an important target for broad-spectrum antibacterial drug

development. The second functional region, the inter-domain binding site, lies between the C-terminal domain (extends between residues 223 and 310) and the H7 helix (**Fig. 1**) [7,8]. Briefly speaking, N-terminal subdomain binds nucleotides while C-terminal subdomain activates GTPase [8], so targeting FtsZ inter-domain site may pave the way for identification specific target. Previous studies have demonstrated two binding pockets for this enzyme, namely the nucleotide-binding pocket associated with GTP/GDP recognition and the interdomain cleft targeted by the well-known inhibitor PC190723 [5]. Extensive and ongoing endeavors have therefore been made on the discovery of FtsZ inhibitors, leading to the identification of diverse inhibitory scaffolds, including naturally derived compounds like Berberine [9] and Sanguinarine [10], along with synthetic GTP mimetics and benzamide-based analogues [11]. Despite recent valuable efforts and advances, the development of promising FtsZ inhibitors into clinically effective and safe antibacterial agents continues to represent a major scientific challenge [5].

Over the last decade, peptides have aroused many enthusiasts as encouraging antibacterial therapies to fight the current growing antimicrobial resistance crisis [12]. The wide and rapid spared of antibiotic resistant agents, including carbapenem-resistant Pseudomonas aeruginosa, and methicillin-resistant Staphylococcus aureus etc., have raised a warning to pressing need for discovery and development novel antibacterial therapeutics [13]. Antimicrobial peptides often induce their mechanism of action through disrupting membrane, which varies from conventional therapeutic agents targeting one bacterial pathway [14]. This important difference bears remarkable benefits and merits, including potential activity against various bacterial pathogens, and multidrug-resistant strains. Astonishingly, peptides postulate superior biocompatibility, and ability to improve human immunity, highlighting their capacity as breakthrough pharmaceuticals[13,14]. These remarkable pharmaceutical features put peptides as a vital threshold in the establishment of novel agents to fight microbial infectious and tackle the increasing spread of antibiotic resistance.

Bovine milk is rich in pharmaceutical proteins like casein and Lactroferrin with promising antibacterial activities [15-18]. Lactoferrin from bovine milk, a glycoprotein of 80 kDa, falls within transferrin family, which was initially extracted from bovine milk [15,19-21]. Lactoferrin ubiquitously exists across mammalian neutrophil granules and secretions, exhibiting

antimicrobial activity and facilitating immune responses, thereby supporting host defense throughout life [22]. This pharmaceutical protein displays diverse bioactivities, e.g., antiviral, anti-inflammatory, antibacterial, immunomodulatory, anticarcinogenic, and antioxidant, and so on [15,23], and especially its antibacterial activities are highlighted numerous reports [24-29]. Surprisingly, recent computational investigations have revealed that mammalian lactoferrins incorporate functional domains such as Tubulin/FtsZ, demonstrating a confomrational relationship with this vital bacterial cell division protein [30]. This point of view was further supported by previous research a novel bovine-derived antimicrobial peptide, F1, efficiently inhibits bacterial proliferation by improving the ClpXP's activity to degrade the cell division proteins FtsZ and ZapC [31]. Since the FtsZ is validated as a vital target for antimicrobial development and peptides are increasingly recognized as promising FtsZ inhibitors [32,33], bovine milk lactoferrin may be of promise as template for the rational design of novel FtsZ-targeting antibacterial agents. Bearing this fact in mind, and given the remarkable role of computational approaches in the fascinating field of drug design and discovery, in this study, for the first time, bovine milk lactoferrin is considered as template to design novel peptides with promising inhibitory potential against FtsZ. To do this, the protein template is docked into the target FtsZ to identify hotpots involved contacts with the FtsZ PC binding site, making the sequence as peptide template. The MD simulations and MM/PBSA calculations will illustrate the prone spots for mutations, which introduction of the mutations to the template leads to a peptide library. The most promising mutant peptides, after docking to the target, are introduced to MD simulations to assess their impacts on FtsZ structure and dynamics.

2. Materials and Methods

2.1. Peptide Library Production

Initially, protein-protein docking was supplemented between the template sequence, bovine lactoferrin (Uniprot: P24627), and the target FtsZ PC binding site using HADDOCK webpage to identify a peptide template of 10 residues. To perform the docking procedure, bovine lactoferrin fasta sequence (Unitpro: P24627) is extracted from Uniprot website, and it is subjected to

AlphaFold2 to generate a valid building block of the protein template (bovine lactoferrin). The generated protein template and the target FtsZ (pdb code: 4DXD) are introduced to HADDOCK website, and finally, the template-target complex belonging to the docking cluster with the lowest HADDOCK score is chosen for subsequent evaluations. Eventually, the peptide template (L62E63C64I65R66A67I68A69E70K71) will be introduced to MD simulations, and residue-wise MM/PBSA energy decomposition is performed to identify potential mutation-prone positions within the peptide sequence (**Table 1**). The possible found mutation spots are introduced to the sequence of peptide to produce to the library of peptide (**Table S1, Supporting Information**). The structures of all peptides have been created via CHIMERA 1.8.1.

2.2. Docking Studies

To assess the inhibitory potential of the designed peptides against FtsZ, their 3D structures are docked against the target PC binding site (FtsZ; pdb code: 4DXD) by HADDOCK website, the resulting peptide–enzyme complex conformations with the most favorable binding energies are chosen for structural analysis.

2.3. Toxicological and Allergenic Assessment

One of the most vital steps in design and development of novel peptide-based inhibitors against FtsZ is to investigate the allergenicity and toxicity since these assessment can ensure the biocompatibility and safety profile of peptide candidates by identifying possible immune responses before future experimental and clinical development. Probable severe immune responses might diminish therapeutic effects and increase the possibility of side effects. Therefore, the allergenicity and toxicity of the designed peptides are assessed through AllerTOP 2.0 and ToxinPred websites because these online platforms use artificial intelligence-based methods to determine peptide sequences with potential safety concerns during preliminary screening.

2.4. Molecular Dynamics (MD) Simulations

MD simulations are supplemented to predict dynamic nature of FtsZ-peptide systems. Simulations are fulfilled via GROMACS version 2024.2, using CHARMM36 force field to generate coordination and topology files of the target protein and peptides. After which, every cubic simulation boxes are filled with water (SPC/E model), maintaining a 1 nm distance between the solute and box edges under periodic boundary conditions. Afterward, the simulation boxes are neutralized by incorporating of enough amounts of counter ions. Energy minimization is further done through steepest decent algorithm until the system energy of below 10 kJ/mol is achieved[34]. The complexes are then equilibrated step at 300 K via the Berendsen thermostat, while the pressure is remained 1 bar pressure under both NVT and NPT equilibration phases. Consequently, 150 ns production phase will be carried out applying the PME (Particle Mesh Ewald) approach to compute long-range electrostatic interactions, whereas the Verlet integration algorithm is used to calculate atomic trajectories. 2D and 3D visualizations are prepared through LigPlot+ 2.3.1 and Discovery Studio 4.5 software.

2.5. Mutations

To assess the effect of mutations on peptide stability, peptide sequences are introduced into the MC-SM platform, a structure-based computational technique for predicting the influence of mutations on molecular stability. In this line, every single amino acid is individually replaced, and the corresponding ΔΔG magnitudes are computed to quantify the variation in free energy relative to the native sequence. These estimations can facilitate the recognition of favorable substitutions capable of improving peptide stability and potentially enhancing biological performance.

$$\Delta\Delta G = \Delta G_{original} - \Delta G_{mutant}$$

The estimations provided by mCSM platform can be explained by calculated changes in free energy, which means the mutations with positive ΔΔG values are considered as favorable

changes leading to increasing the stability of the peptide. However, replacements with negative ΔΔG magnitudes associate with reduced structural stability. In contrast, ΔΔG values close to zero suggest that the introduced amino acid changes may have a minimal effect on the overall energetic profile.

3. Results and Discussion

3.1. Molecular docking studies

FtsZ is recognized as an ideal target for novel antibacterial drug development since inhibition of this enzyme can hinder successful cell proliferation, and also, despite the broad conservation of FtsZ in different bacterial strains, no homologous protein is present in eukaryotic organisms, and its amino acid sequence shares only limited identity with tubulin. Thus, this significant biological distinction improves its capacity as a therapeutic target. Despite recent valuable efforts and advances, the development of promising FtsZ inhibitors into clinically effective and safe antibacterial agents continues to represent a major scientific challenge [5]. As it was mentioned earlier, lactoferrin has been shown potent antibacterial potential; thus, this piece of fact has prompted us to shed light on the lactoferrin-derived peptides as promising therapeutic agents against FtsZ. Extensive and ongoing endeavors have therefore been made on the discovery of FtsZ inhibitors, leading to the identification of diverse inhibitory scaffolds, including naturally derived compounds like Berberine [9] and Sanguinarine [10], along with synthetic GTP mimetics and benzamide-based analogues [11]. Despite recent valuable efforts and advances, the development of promising FtsZ inhibitors into clinically effective and safe antibacterial agents continues to represent a major scientific challenge [5].

Structurally speaking, FtsZ contains two ligand-binding pockets: the nucleotide-binding domain and the inter-domain cleft [7,8]. The nucleotide-binding pocket, located in the N-terminal subdomain (form residues 13 to 173) (**Fig. 1**), regulates GTP binding and hydrolysis, controlling protofilament assembly and bacterial cytokinesis [7,8]. Since this region is highly conserved across bacterial species, it represents an important target for broad-spectrum antibacterial drug development. The second functional region, the inter-domain binding site, lies between the C-

terminal domain (extends between residues 223 and 310) and the H7 helix (**Fig. 1**) [7,8]. Briefly speaking, N-terminal subdomain binds nucleotides while C-terminal subdomain activates GTPase [8], so targeting FtsZ inter-domain site may pave the way for identification specific target.

Previous studies have demonstrated two binding pockets for this enzyme, namely the nucleotide-binding pocket associated with GTP/GDP recognition and the interdomain cleft targeted by the well-known inhibitor PC190723 [5]. Hence, in this study, our peptide design are inspired by the interaction profile of PC190723 because this interaction profile cover the necessary amino acid residues required for the enzymatic profile of the target protein, paving the way for exploring novel inhibitors for FtsZ with promising potential. To initiate our computational workflow, the 3D building blocks of the target FtsZ and the modelled template (lactoferrin) are subjected to HADDOCK online webserver to find a peptide template of 10 amino acid sequence. The protein-protein docking have indicated a binding affinity of -73.0 kcal/mol. Surprisingly, the interaction profile of the complex demonstrates almost 60 no-polar/polar interactions are established between the templated and the residues located almost at the interdomain cleft, which resembles the docking profile of inhibitor PC190723. More interestingly, roughly one-third these interactions (~20 polar/non-polar contacts) are formed by the amino acid residues between 62-70 of the lactoferrin template, and among these interactions, hydrogen bonding and hydrophobic contacts with residue numbers ser204, Gly205, Glu206, and Val207 are important. Hence, the sequence region from 62-71 of lactoferrin is chosen as our peptide template (**Fig. 2**).

Consequently, a 10-length peptide template (L62E63C64I65R66A67I68A69E70K71) is generated and introduced into MD simulations with FtsZ, and MM/PBSA calculations are carried out to identify mutation-prone residues. As it is exhibited in **Table 1**, the residues I65, A69, and E70 demonstrate positive binding free energy values, proposing that the mentioned residues may bring about weak and destabilizing impacts on the total binding affinity of the peptide–protein complex. This means that replacement of the amino acid sequence with a less favorable energetic contribution can provide a suitable way for improving weak molecular interactions, strengthening the total binding free energy of the complex. Therefore, the recognized hotspots (I65, A69, and E70) are introduced into the mCSM website to search for favorable substitutions that lead to improving the total binding energy of the peptide template. This online framework

apply ΔΔG-based analysis to assess residue replacement and predict their effects on binding free energy. Positive ΔΔG magnitudes may highlight stabilizing impacts of the predicted mutations. Afterward, peptide variants with favorable residues at each spot are combined to assess their binding affinities against the FtsZ. Finally, when the potential mutations are found, and the amino acid substitutions are introduced into the template, a peptide library of 144 peptides is prepared though CHIMERA 1.8.1. After that, allergenicity and toxicity of the library members are screened through AllerTop 2.0, and ToxinPred websites. To the best of our knowledge, almost half of the peptide library (71 peptides) are predicted to have a safe profile (**Table 2**). At last, the peptides with safe profile are subjected to the HAADDOCK website to discover their binding affinity against the target protein; FtsZ. Consequently, these peptides have been introduced to the HADDOCK platform to uncover their inhibitory potency versus FtsZ binding site. In the following section, the molecular docking results of the peptides with superior affinities toward FtsZ are discussed in detail.

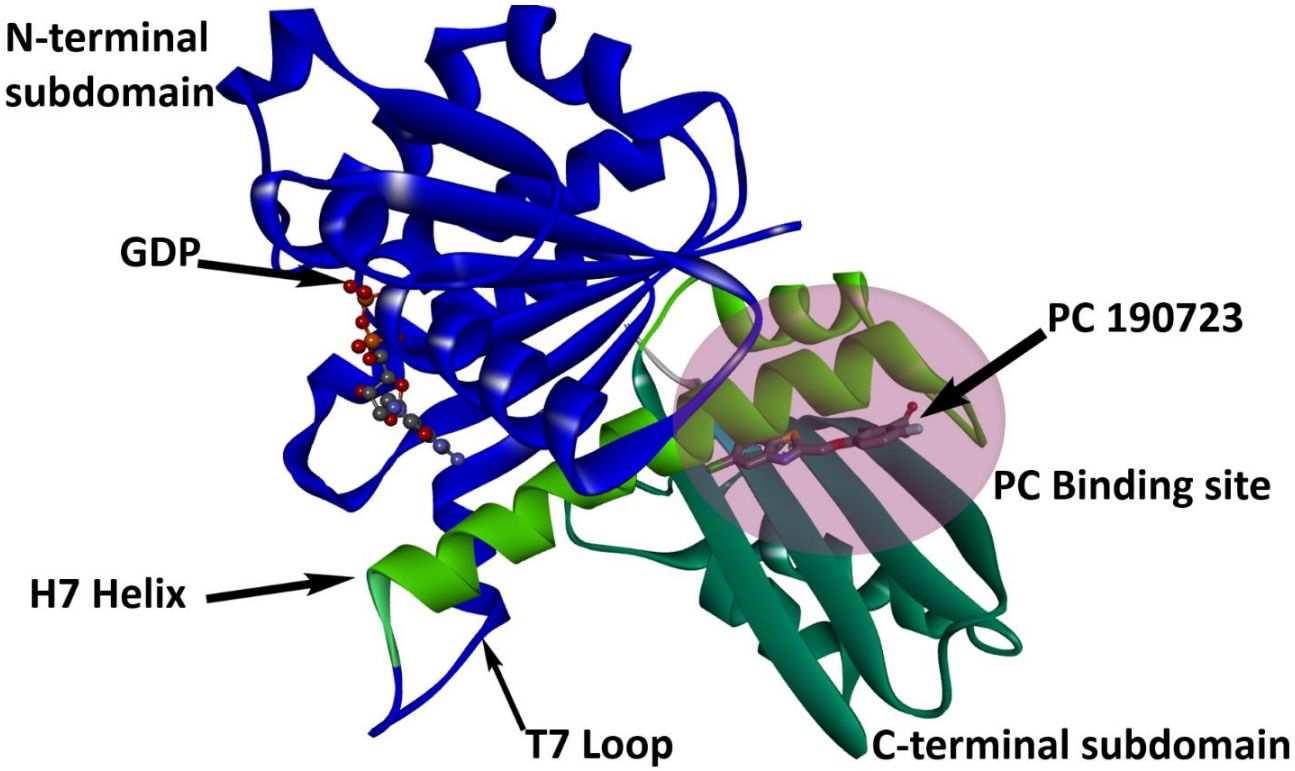


Figure 1. The 3D representation of the building block of *S. aureus* FtsZ (PDB code: 4DXD). The N-terminal (colored in dark blue; residues from 13-173) is connected to the C-terminal domain (colored in green; extends between residues 223 and 310) by H7 helix (colored in light green). FtsZ possesses two main ligand-binding pockets: the conserved N-terminal nucleotide-binding pocket responsible for GTP binding, and the interdomain cleft located between the C-terminal domain and H7 helix, associated with GTPase activation and selective inhibitor binding. The PC binding site, is highlighted in purple, as the interdomain cleft is targeted by the inhibitor PC190723.

Table 1. Binding Free Energy estimation of the peptide template against FtsZ by MM/PBSA approach.

Residue Number	MM/PBSA Energy
L62	-85.835
E63	-23.335
C64	-4.266
I65	5.09
R66	-59.887
A67	-444.996
I68	-2.806
A69	0.093
E70	1.892
K71	-48.545

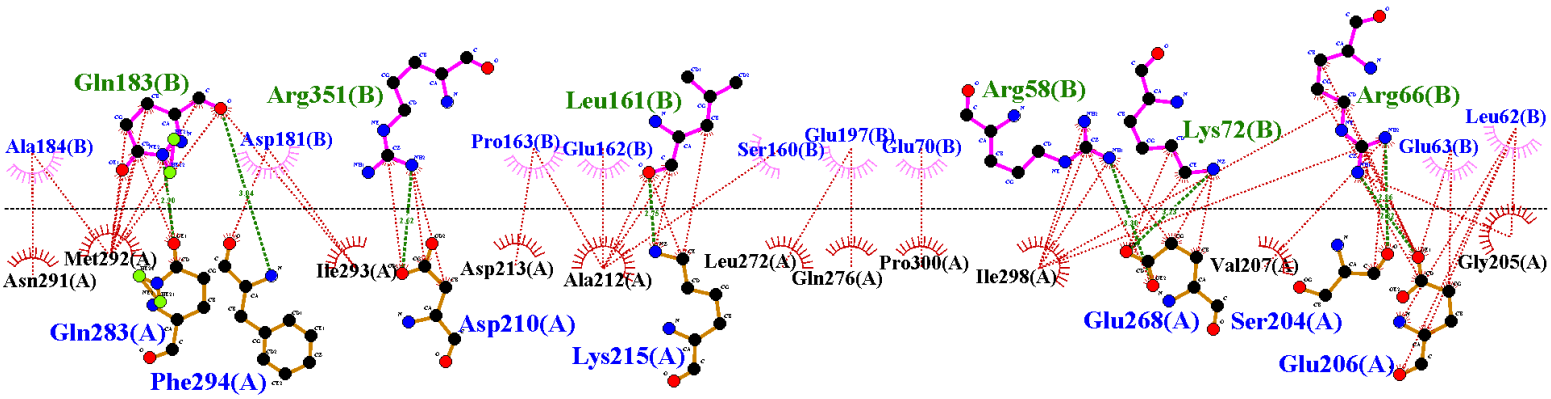


Figure 2. The schematic representation of polar/nonpolar contacts of the bovine milk lactoferrin with the FtsZ, illustrating efficient binding to the interdomain celft FtsZ, mimicking the binding profile of inhibitor PC190723. The modelled conformation of the template and FtsZ are subjected to HADDOCK online platdorm to find a peptide template of 10-length sequence. Protein-protein docking revealed a binding affinity of -73.0 kcal/mol, with ~60 polar/non-polar contacts concentrated at the interdomain cleft — a profile resembling that of the inhibitor PC190723. Roughly one-third of these contacts originate from

lactoferrin residues 62-70, with key hydrogen bonding and hydrophobic interactions at Ser204, Gly205, Glu206, and Val207, identifying residues 62-71 as the selected peptide template.

Table 2 .Molecular docking evaluations of the mutant peptides with safe profile with FtsZ by HADDOCK online framework.

Peptide No.	PEP sequence	Docking Score	VdW energy	Elec Energy	Desolvation energy
TEMPLATE	LECIRAIAEK	**-63.1**	-38.9	-121.3	-1.8
PEP1	LECWRAIWVK	-56.1	-29.7	-129.0	-14.6
PEP2	LECFRAIWVK	-56.5	-22.2	-154.2	-15.4
PEP3	LECFRAIWPK	-61.5	-37.0	-104.9	-13.8
PEP4	LECHRAIWHK	-52.8	-29.9	-192.5	-7.4
PEP5	LECHRAIWMK	-53.6	-34.2	-91.5	-17.1
PEP6	LECWRAIEVK	-51.1	-32.3	-120.1	-6.8
PEP7	LECWRAIELK	-49.6	-21.3	-145.4	-10.3
PEP8	LECWRAIEPK	-49.6	-27.1	-172.7	-6.4
PEP9	LECFRAIEIK	-61.9	-35.2	-126.2	-11.6
PEP10	LECHRAIEVK	-48.6	-33.7	-132.2	2.6
PEP11	LECHRAIELK	-36.2	-30.4	-84.8	-1.0
PEP12	LECWRAIEIK	-54.9	-30.8	-170.2	-8.8
PEP13	LECFRAIEVK	-66.4	-36.5	-127.3	-11.3
PEP14	LECFRAIELK	-66.4	-39.6	-124.8	-11.7
PEP15	LECFRAIEPK	-61.5	-37.3	-121.7	-11.2
PEP16	LECHRAIEIK	-39.0	-27.4	-115.7	-0.8
PEP17	LECHRAIEMK	-67.6	-41.1	-177.5	-0.4
PEP18	LECWRAICLK	-51.1	-21.1	-147.0	-10.9
PEP19	LECFRAICHK	-65.0	-37.7	-128.0	-13.1
PEP20	LECFRAICMK	-69.7	-38.8	-136.6	-12.3
PEP21	LECHRAICPK	-59.1	-35.9	-173.3	-4.9
PEP22	LECWRAICIK	-61.5	-32.6	-167.6	-11.7
PEP23	LECWRAICHK	-58.4	-30.3	-181.7	-12.6
PEP24	LECWRAICMK	-56.6	-34.6	-147.9	-10.4
PEP25	LECHRAICHK	-48.1	-31.3	-119.3	-6.8
PEP26	LECHRAICMK	-67.9	-36.4	-174.7	-5.8
PEP27	LECWRAIDVK	-56.6	-29.6	-175.6	-8.6
PEP28	LECWRAIDLK	-49.5	-35.1	-82.7	-9.6
PEP29	LECWRAIDPK	-42.4	-30.9	-98.9	-6.8
PEP30	LECFRAIDIK	-60.6	-36.2	-116.7	-11.3
PEP31	LECHRAIDVK	-48.6	-36.9	-135.1	3.1
PEP32	LECHRAIDLK	-45.5	-25.0	-155.1	-2.3
PEP33	LECHRAIDPK	-42.6	-33.0	-120.0	1.7
PEP34	LECWRAIDIK	-58.7	-30.0	-165.4	-9.4
PEP35	LECFRAIDPK	-63.2	-36.9	-119.8	-11.2

PEP36	LECHRAIDIK	-37.0	-25.5	-118.6	2.4
PEP37	LECHRAIDHK	-52.9	-36.7	-136.0	-2.7
PEP38	LECHRAIDMK	-41.6	-31.8	-128.6	5.2
PEP39	LECWRAIFVK	-55.5	-24.5	-115.2	-19.1
PEP40	LECFRAIFIK	**-73.0**	-44.2	-96.7	-23.2
PEP41	LECHRAIFVK	-53.9	-34.5	-141.9	-0.6
PEP42	LECHRAIFLK	-48.1	-25.3	-107.3	-10.6
PEP43	LECWRAIFIK	-53.7	-21.9	-120.7	-18.5
PEP44	LECFRAIFVK	**-74.6**	-43.5	-85.4	-24.5
PEP45	LECHRAIFIK	-50.4	-29.5	-134.1	-0.9
PEP46	LECHRAIFMK	-42.7	-30.7	-108.7	-1.0
PEP47	LECWRAIHLK	-53.9	-28.6	-170.0	-12.4
PEP48	LECHRAIHVK	-53.4	-34.4	-99.2	-12.1
PEP49	LECHRAIHLK	-65.0	-37.8	-121.5	-11.1
PEP50	LECWRAIHIK	-50.5	-29.3	-164.1	-9.5
PEP51	LECFRAIHVK	-68.6	-37.9	-126.4	-16.0
PEP52	LECHRAIHIK	-49.5	-30.8	-150.5	-4.1
PEP53	LECHRAIHHK	-55.4	-25.4	-203.8	-3.7
PEP54	LECHRAIHMK	-39.8	-28.1	-114.6	-2.2
PEP55	LECWRAIMVK	-52.5	-27.5	-167.9	-9.3
PEP56	LECFRAIMIK	**-73.5**	-37.8	-149.3	-12.3
PEP57	LECHRAIMVK	-49.5	-25.9	-169.7	-2.4
PEP58	LECHRAIMLK	**-75.2**	-42.7	-171.0	-5.7
PEP59	LECWRAIMIK	-58.5	-28.8	-169.0	-11.4
PEP60	LECFRAIMVK	-64.1	-38.3	-142.8	-12.2
PEP61	LECHRAIMIK	-48.9	-35.1	-105.9	-6.6
PEP62	LECHRAIMMK	-38.0	-28.4	-97.9	-3.9
PEP63	LECWRAIYVK	-53.5	-33.2	-136.3	-4.6
PEP64	LECWRAIYLK	-51.9	-29.9	-121.7	-11.1
PEP65	LECHRAIYVK	-54.3	-37.1	-129.9	-0.4
PEP66	LECHRAIYLK	-57.3	-28.3	-205.6	-3.3
PEP67	LECWRAIYIK	-53.9	-26.8	-110.9	-14.2
PEP68	LECWRAIYMK	-49.5	-29.7	-109.8	-5.0
PEP69	LECHRAIYIK	-41.3	-28.0	-119.3	-4.7
PEP70	LECHRAIYHK	-51.0	-21.6	-222.6	-3.0
PEP71	LECHRAIYMK	-49.4	-33.0	-127.0	-0.4

3.1.1. The effect of residue substitutions on binding affinity to FtsZ:

Based on our molecular docking findings, 4 out of 71 peptides, including PEP40, PEP44, PEP56, and PEP58, are estimated to have superior binding affinities of -73.0, -74.6, -73.5, and -75.2

kcal/mol to the target protein. It is interesting to note that the four mutant peptides demonstrate a meaningful stronger binding affinities to FtsZ in comparison to the peptide template (-63.1 kcal/mol). The sequences of the superior peptides are as follow:

- PEP40 (L62E63C64I65R66A67I68A69E70K71) –> LEC**F**RAI**FI**K): I65F, A69F, E70I; -73.0
- PEP44 (L62E63C64I65R66A67I68A69E70K71) –> LEC**F**RAI**FV**K): I65F, A69F, E70V; -74.6
- PEP56 (L62E63C64I65R66A67I68A69E70K71) –> LEC**F**RAI**MI**K): I65F, A69M, E70I; -73.1
- PEP58 (L62E63C64I65R66A67I68A69E70K71) –> LEC**H**RAI**ML**K): I65H, A69M, E70L; -75.2

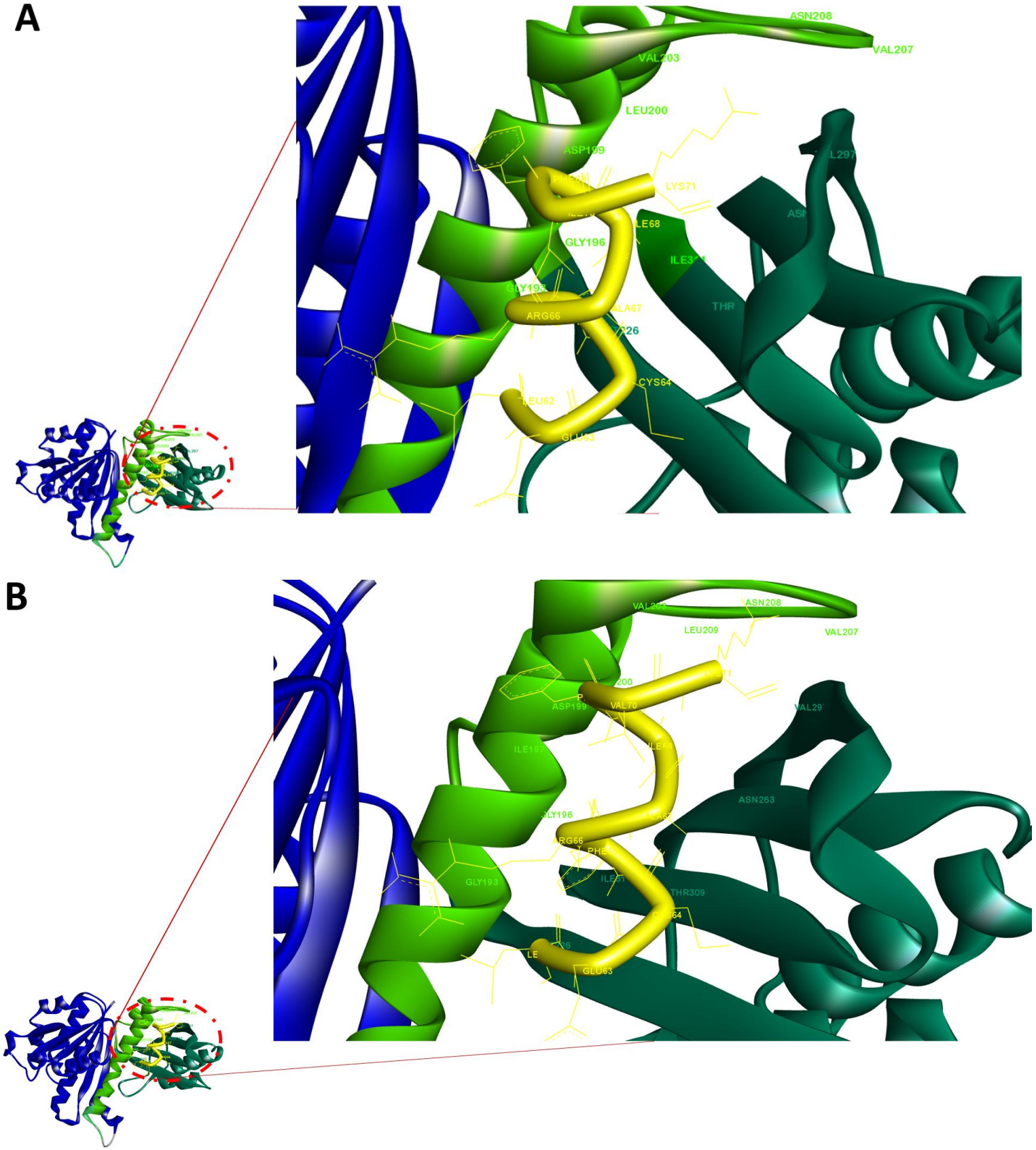
Further assessment of the interaction profile of the chosen peptides with the target enzyme uncover interesting notes. Comparative considerations of peptide-protein systems highlight the marked role of residue displacement on the binding affinities of the superior mutant peptides since the four peptides have benefited from residue substitutions that generally enhanced the pocket occupancy and hydrophobic complementarity. However, the extent of this improvement varies marginally among these mutant peptides. For example, PEP58 demonstrates superior binding energy of -75.2 kcal/mol, which has almost ~12 kcal/mol stronger binding affinity to the target protein compared to that of the template (-63.1 kcal). This actually highlights the substantial role of residue substitutions. Following this, PEP44 displayed the strongest binding affinity (−74.6 kcal/mol), followed by PEP56 (−73.5 kcal/mol) and PEP40 (−73.0 kcal/mol). In general, I65F/A69F/E70V substitution pattern produced the most favorable interaction profile. According to these results, it should be noted that although introducing a bulky aromatic side chains such as phenylalanine (in PEP40, PEP48, PEP56) instead of smaller, polar residue like isoleucine (I65) in the proximity of the N-terminal makes the capability of peptide to bind, if I65 is replaced with histidine the potency becomes stronger; like in PEP58 compared to other three peptides. The reason might lie in the slightly better potential of phenylalanine in engagement with hydrophobic contacts. This can be seen in the interaction profile of PEP58; H65 makes 7 non-polar contacts, while F65 in other three peptide has established marginally lower (5-6) hydrophobic interactions with the target residues.

Interestingly, as for mutations of A69, substitution of a little bulkier amino acid (such as phenylalanine in PEP58 or methionine in PEP48) near the C-terminal can improve the binding affinity. Last but not least, replacement of glutamic acid (E70; as a negatively charged, polar

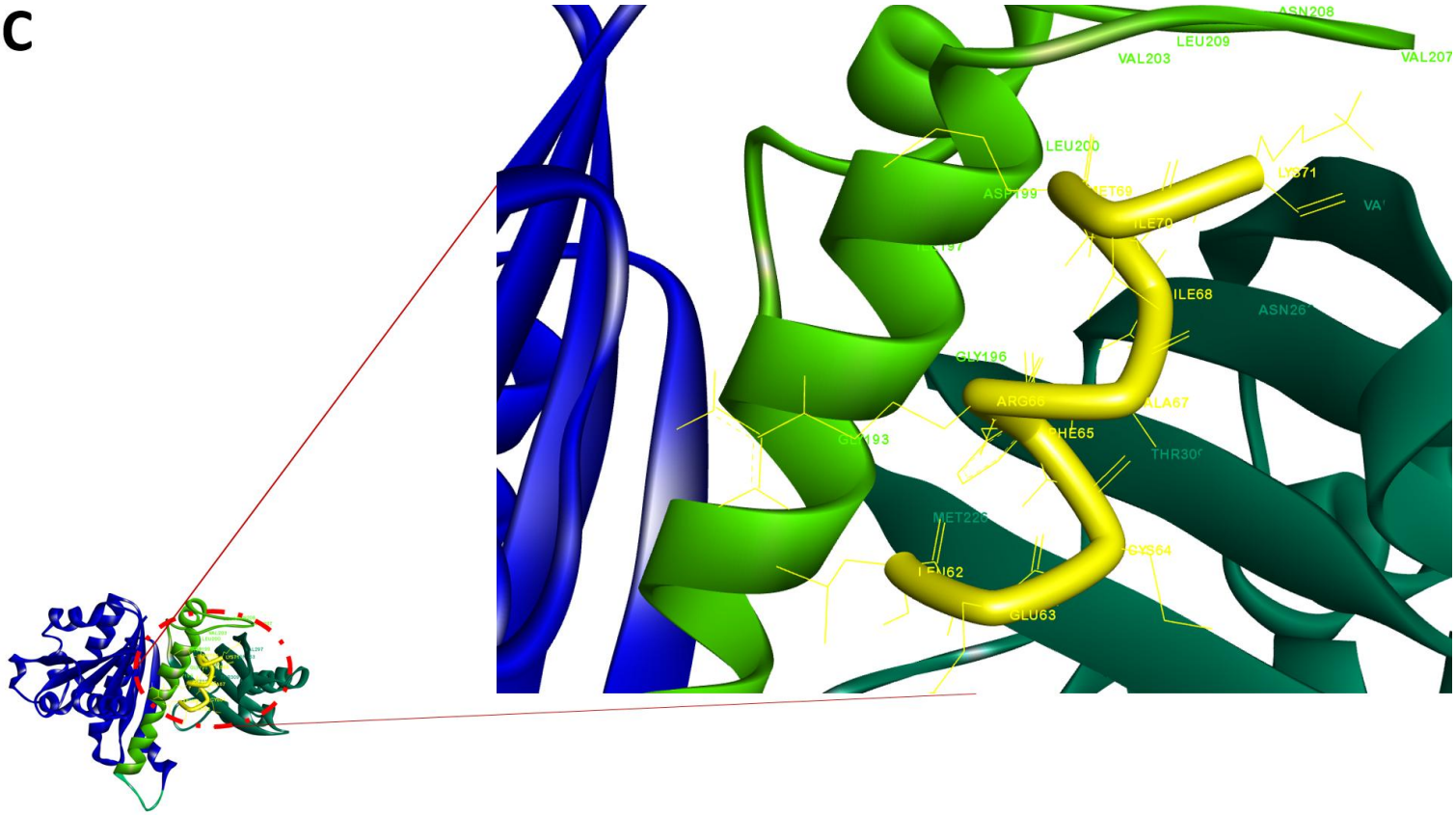
residue) with isoleucine has made the binding affinity weaker, as seen in PEP40 and PEP56, since by this substitution the side chain changes from a long, negatively charged carboxylate group to a bulky, nonpolar aliphatic group. This substitution eliminates the electrostatic interactions that originally stabilizes the peptide–protein complex. However, if this residue is replaced either with valine (like in PEP58) or with leucine (like in PEP44), the binding affinity is improved because these two residues have a smaller, hydrophobic side chains that facilitate hydrophobic contacts within the binding interface, whereas isoleucine may cause steric clashes or suboptimal orientation.

3.2.2. Interaction profile of each peptide-target complex

In PDB 4DXD, PC190723 binds to the interdomain cleft of *Staphylococcus aureus* FtsZ, which represents an allosteric and non-catalytic pocket named PC binding site, rather than the GTPase active site. The binding cleft is surrounded by residues Gly193, Gly196, Ile197, Asp199, Leu200, Val203, Val207, Asn208, Leu209, Met226, Asn263, Val297, Thr309, and Ile311, which collectively generate the core interaction network that accommodates the inhibitor in this allosteric binding site. PC190723 stabilizes the T-state (open conformation) of FtsZ and thereby disrupts polymerization by stabilizing the high-affinity protofilament state rather than directly inhibiting GTP hydrolysis [35-37]. In this study, we focused on this allosteric PC binding site to explore if our designed peptides have the possible potential to mimic the binding profile of this promising inhibitor. As is illustrated in **Fig. 4**, in general, it can be interpreted that all of the selected peptides demonstrate good ability to mimic the binding profile of the inhibitor PC190723. Furthermore, the two mutant peptides, named PEP44 and PEP58, reveal the most promising binding energy to the target enzyme. Although it is often shown that the higher the number of contacts, the stronger binding affinity[38-41], number of contacts caused by our peptide follows PEP58 > PEP40 > PEP56 > PEP44, while binding affinity follows PEP58 > PEP44 > PEP56 > PEP40. This is an interesting observation because a higher number of contacts between peptide and the target often contributes to stronger binding, while the binding affinity observed for these peptides indicates that interaction quality is more


A
ASN208
VAL207
VAL203
LEU200
ASP199
LYS71
LE68
GLY196
ILE3
GLY193
ARG66
LA67
THR
26
CYS64
LEU62
GLU63
B
VAL
ASN208
LEU209
VAL207
200
ASP199
VAL70
VAL29
ILE197
ASN263
GLY196
RG66
PHE
GLY193
ILE
THR309
64
GLU63

C


ASN208
LEU209
VAL203
VAL207
LEU200
LYS71
ILE70
ILE68
GLY196
ALA67
PHE65
THR30
MET226
CYS64
LEU62
GLU63

D

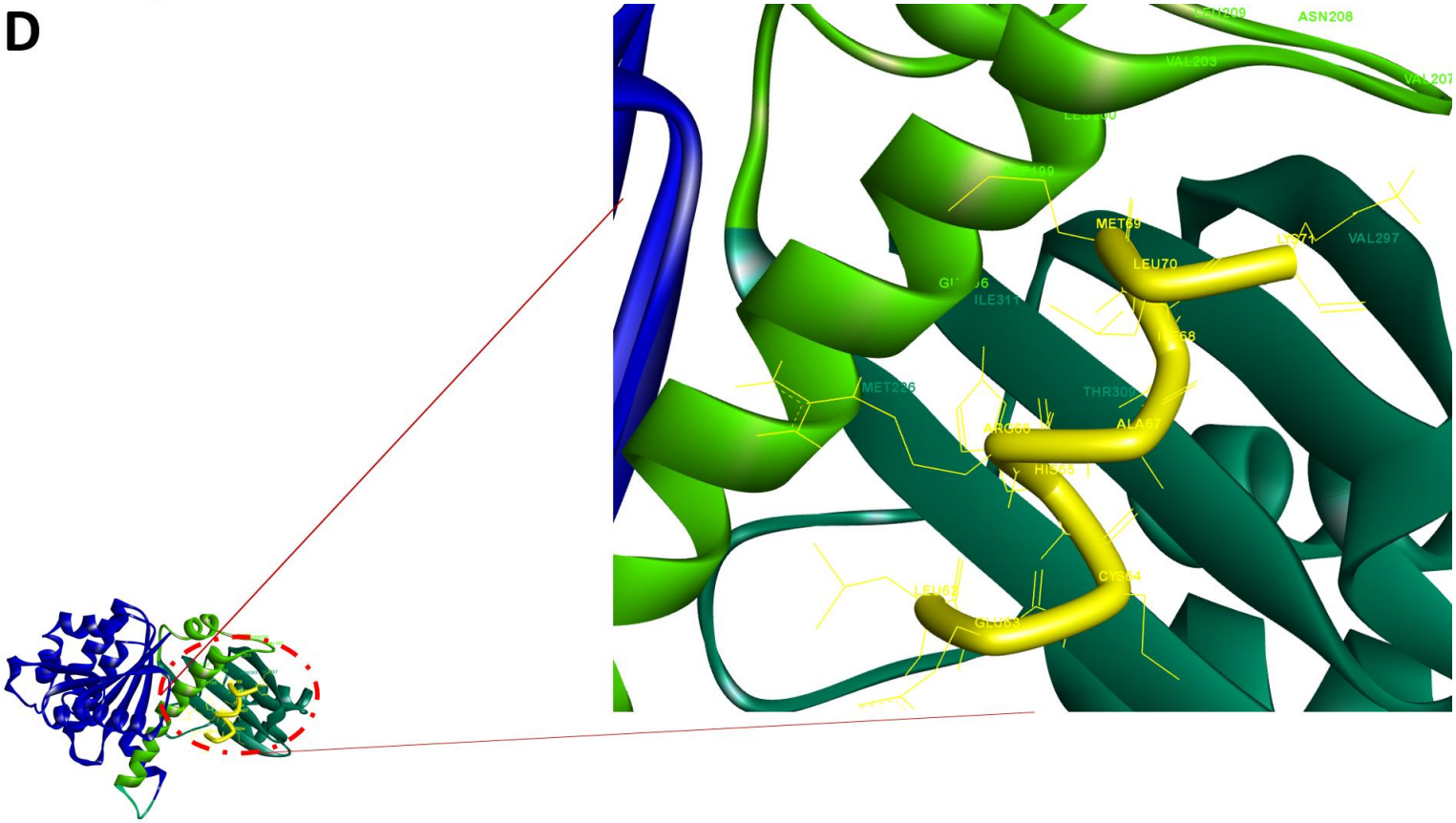
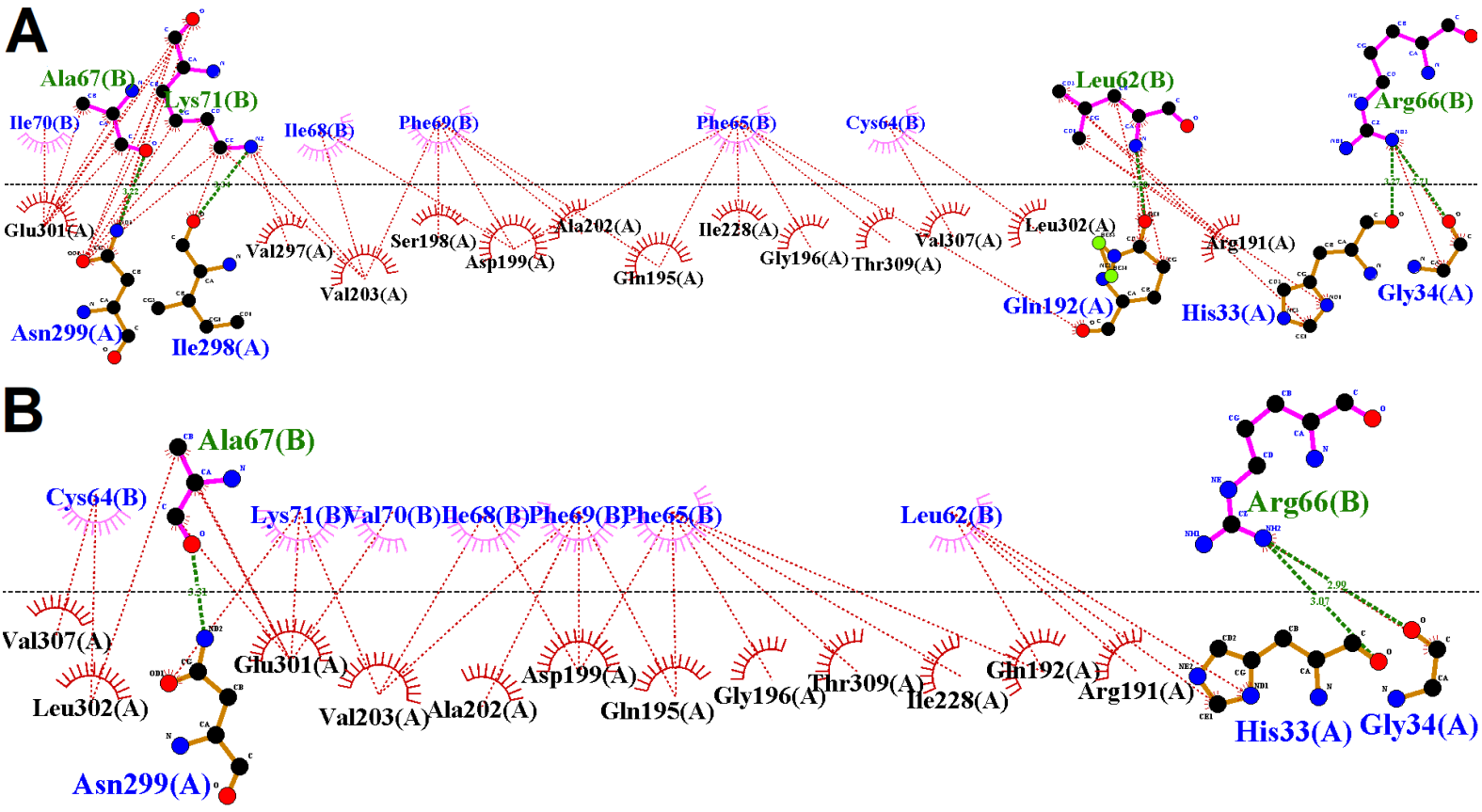

ASN208
VAL203
MET69
LEU70
VAL297
ILE68
MET226
THR30
ALA67
CYS64

Figure 3. 3D illustrations of A) PEP40, B) PEP44, C) PEP56, and D) PEP58 with the binding pocket of the target protein.

vital than contact quantity alone. For example, PEP58 exhibited the highest affinity and the greatest number of contacts, likely due to enhanced hydrophobic packing resulting from the I65H, A69M, and E70L substitutions. However, PEP44, with fewer contacts, showed stronger binding than PEP40 and PEP56, proposing that its interactions are more energetically favorable, possibly through optimized hydrophobic interactions and better accommodation within the FtsZ binding pocket. Thus, the strength, geometry, and energetic contribution of individual contacts, rather than the total number of interactions, primarily determine peptide–FtsZ binding affinity.



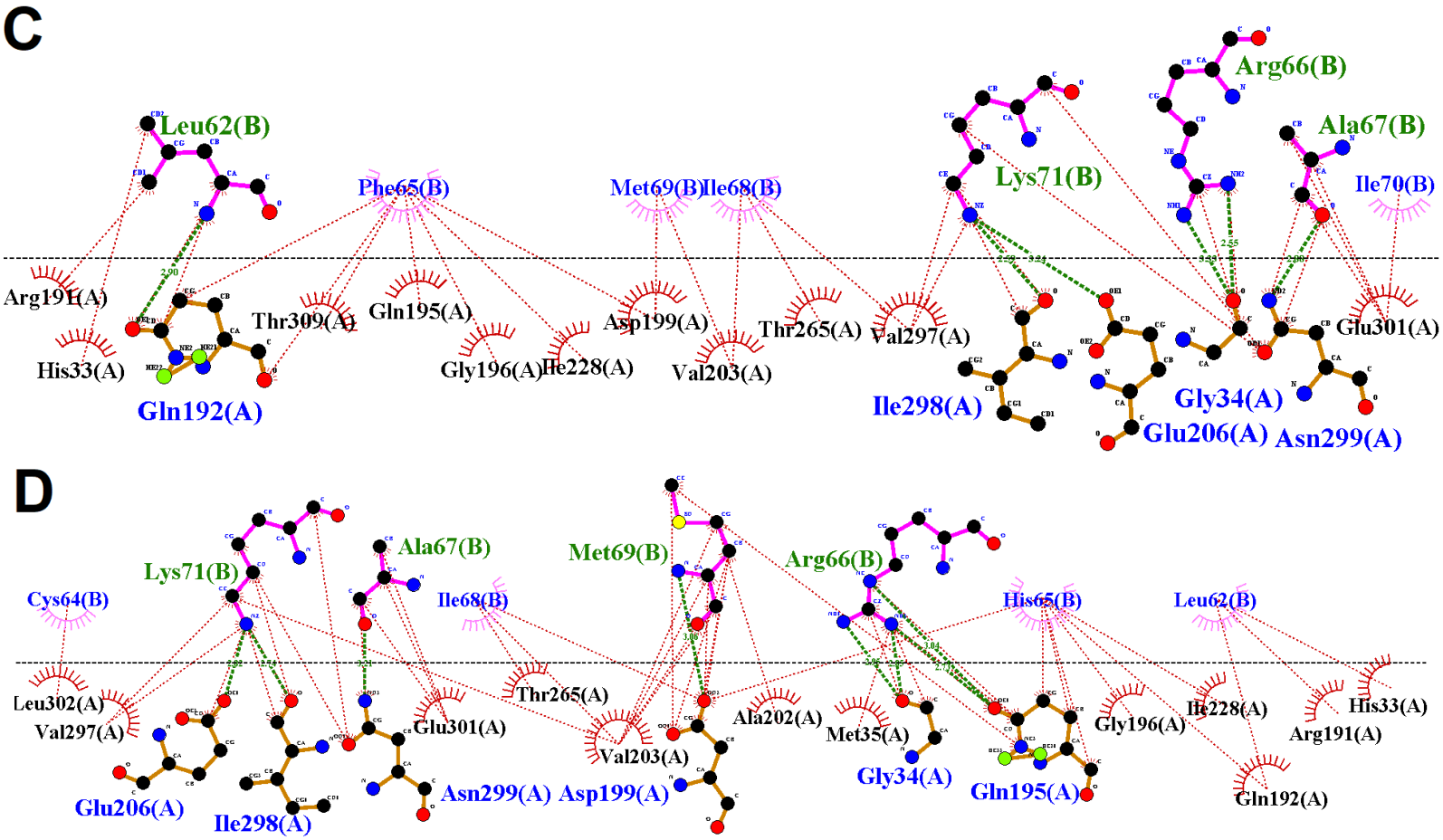


Figure 4. 2D exhibitions of A) PEP40, B) PEP44, C) PEP56, and D) PEP58 with the binding pocket of the target protein. All four mutant peptides dock into hydrophobic interdomain cleft, sharing 4–5 contact residues with the inhibitor PC190723. PEP58 shows the highest binding affinity through interaction quality (H65/M69-driven hydrophobic packing), not contact count—PEP44 matches it with far fewer contacts via dual phenylalanine anchoring, while PEP40/PEP56 form more contacts yet bind more weakly. Contact geometry, governs affinity, supporting these peptides' potential to allosterically disrupt FtsZ polymerization (see **Table 3** for more details).

Besides, PEP58, with ~50 polar/nonpolar interactions, have superior specificity to the target protein compared to that of PEP44 (with 28 contacts), highlighting the superior residue displacement in PEP58. In PEP44, although positioning two bulky phenylalanine residues at positions 65 and 69 may enhance the binding affinity, replacement of valine, as a slightly bulkier residue at position 70, near the C-terminal has failed to make the binding energy of this peptide

stronger when compared to PEP58. However, as it was mentioned earlier, displacement of histidine at position 65 off the N-terminal, and also, introducing one methionine (M69) as a relatively bulky hydrophobic residue, at the C-terminal improved the binding affinity of PEP58 compared to PEP44 since these two residues can promote the potential of this peptide in formation of nonpolar interactions with the residues located at the PC binding site since this peptide form almost 50 polar/nonpolar contacts with the target. Among which, H65 and M69 of this peptide establish 14 hydrophobic contacts, along with one hydrogen bond with Gln192, Gly196, Gln195, Val203, Asp199, Ala202, Val203. This observation may support the fundamental role of residue displacement in improving binding affinity of PEP58, and enhancing its potential in mimicking the interaction profile of PC190723 by facilitating the peptide conformation through the PC binding site of FtsZ. Besides, the E70L in PEP58 suggests that it would be better to put a slightly bulky, longer hydrophobic chain residue like leucine near the C-terminal instead of either isoleucine (like in PEP40 and PEP56) or valine (like in PEP44), since maybe leucine can better accommodate the peptide conformation in the PC binding site of FtsZ, enhancing binding affinity. PEP58 has also involved in roughly 7 more polar contacts and more nonpolar interactions through L62, R66, A67, and K71 with residue numbers 33-35, 191, 195, 196, 199, 203, 206, 298, 299, 297, 301, 302. These interactions highlight the supreme potential of PEP58 to simulate the binding profile of PC190723 since this peptide involved in interactions with the interdomain cleft (residue numbers form 199-209).

In terms of interaction profile, PEP58 also make the highest number of hydrogen bonds (8) compared to PEP44 with just three polar contacts. Although polar interactions often fortify the binding affinity, the hydrogen bond formations could not guarantee the superiority of binding energies of PEP40 (5) and PEP56 (6) in comparison to PEP44.

As for binding pattern of PEP44, this peptide is bound to the FtsZ interdomain cleft through basically 25 hydrophobic and 3 polar interactions with residues roughly at the core of H7 helix; situating near or at the interdomain cleft such as residues His33, Gly34, Gly192, Arg191, Gln195, Gly196, Asp199, Ala202, Val203, Ile228, Asn299, Glu301, Leu302, Val307, and Thr309. Interestingly, approximately 90% of the contacts with the target is governed by hydrophobic contacts, revealing that substitution of Ile65 and Ala69 with phenylalanine, and replacing Glu70

with valine provided extensive hydrophobic contacts for anchoring to the interdomain cleft of the target, explaining its supreme binding affinity of PEP44 relative to PEP40 and PEP56 (even with higher number of polar contacts).

Underlying the other two peptide, PEP40 and PEP56 displayed comparable but slightly weaker binding affinities toward FtsZ (−73.0 and −73.5 kcal/mol), indicating that both peptides maintain favorable interactions within the binding cleft, while their stabilization mechanisms differ. PEP40 and PEP56 establish 5 and 6 H-bonds, and total contact number of 35 and 43 with the target although their binding affinities could not surpass PEP44 and PEP58. Regardless of higher number of contacts and polar interactions, their lower binding affinities compared to PEP44, might be linked with some less energetically favorable contacts, negatively affecting the accommodation of their conformations into the FtsZ binding pocket.

In PEP40, incorporating two bulky phenylalanine to positions 65 and 69 enhanced van der Waals packing and π-mediated interactions with hydrophobic regions of FtsZ, improving pocket complementarity. The significant role of these two phenylalanine are highlighted when comparing the hydrophobic contacts of PEP40 (38) with that of PEP56 (29). Furthermore, the E70I substitution eliminates the negatively charged glutamate residue and, facilitate its accommodation in the nonpolar environment of the binding site. The interaction profile of PEP40 supports this interpretation, as the peptide forms multiple hydrogen bonds with His33, Ile298, Asn299, Gln192, His33, and Gly34, accompanied by extensive hydrophobic contacts involving Val297, Ala202, Val203, Ile225, Gly196, Leu302, Thr350, and Ala307. The presence of both polar anchoring interactions and broad hydrophobic stabilization contributes to make its binding affinity comparable to the template (-63.1 kcal/mol), while still failed to surpass binding energies of PEP44 and PEP48. Similarly, PEP56 is bound to the interdomain cleft of the target with similar binding affinity of -73.5 kcal/mol, which benefits from the I65F and E70I substitutions, which enhance aromatic interactions within the binding pocket. Unlike PEP58, introducing one methionine, as a bulky hydrophobic sulfur-containing side chain without the aromatic ring, at position 69 does not guarantee the improvement of binding affinity. Although methionine improves hydrophobic occupancy, its interaction share is possibly less pronounced than the phenylalanine-mediated stabilization observed in PEP40. PEP56 involves in total 35

polar/nonpolar interactions; including 6 H-bonds with Gly34, Arg191, Glu206, Ile298, Asn299; and 29 hydrophobic contacts with His33, Gln192 , Gln195, Gly196, Asp199, Ile228, Thr265, Val297, Glu301, Thr309, Thr265, Val203. This interaction profile demonstrates a stable interaction network that supports its good binding affinity (compared to the template).

To check the specificity of each peptide toward FtsZ, all of the residues engaged in contacts with the four peptides are listed in **Table 3**. It can be seen that PEP58 and PEP40 establish contact with 18 residues, followed by PEP56 and PEP44 that are involved in contacts with 16 and 15 residues, respectively. Among these contacts, highlighted residues in blue (see **Table 3**) are in common in interaction profile of four peptides, which highlight some similarity in their binding patterns, still with important differences that distinguish their affinity and specificity toward the target FtsZ. It is also asserted that a greater network of contact spots might improve the total affinity, leading to improving the specificity, letting the peptide inhibitor to efficiently distinct from competing ligands and enhance selectivity. This is why PEP58 with a larger contact network possesses higher binding affinity.

As it was pointed out, our peptides hopefully designed to mimic the PC190723 binding profile; interestingly, all of the four mutant peptides are bound to the same hydrophobic PC binding site with 4-5 contact spots (see underlined residues in **Table 3**) in common with the PC190723 binding profile. Strikingly, these results postulate that the designed peptides have promising potential to mimic the binding paradigm of the inhibitor, addressing their good specificity toward the target. Of course, PEP58 has also formed interaction with more residues Met35 and Thr365 that cannot be seen in the contact profile of the other three peptides, which makes its binding profile unique among all designed peptides, while PEP40 contacted with just one residue (Ser198). In total, binding profile of the four peptides can demonstrate that the four peptides are generally bound to the FtsZ interdomain cleft, showing incredible simulating potential to mimic the binding profile of PC190723.

It has previously revealed that residues located at the PC190723 binding site and the interdomain cleft of FtsZ establish an allosteric drug-binding pocket, not the GTP-binding catalytic site. This cleft lies between the two FtsZ subdomains and is built mainly by the H7 helix, the T7 loop, and

nearby residues of the central core, so it acts as a structural hinge that regulates the open/closed conformational state of FtsZ [37,42]. Functionally, these residues are important because they help regulate FtsZ polymerization, filament stability, and Z-ring assembly. When PC190723 binds in this cleft, it stabilizes FtsZ filaments/open conformations, changes filament dynamics, and can reduce productive cell-division function, which is why this pocket is a major antibacterial target [42]. Armed with our molecular docking results, it is predicted that our peptides are bound to the PC190723/interdomain cleft region. Although PEP58 and PEP44 have shown a moderately superior binding energies to target, PEP40 and PEP56 establish strong complexes with the FtsZ with good capability of mimicking PC190723 binding profile since these two peptides have five contacting residues in common with the inhibitor. Thus, the binding of these peptide to this site can cause an allosteric effect rather than a direct blocker of the GTP-binding catalytic pocket. This means these peptides may have the potential to disturb the conformational switching FtsZ needs for normal filament dynamics and Z-ring assembly, and indirectly impair its GTPase activity required for bacterial cell division.

Table 3. Residue-level contacts between each peptide and FtsZ are summarized. Parenthetical values denote hydrogen-bonding residues, while all remaining listed residues indicate hydrophobic interactions.

Peptide No.	**The FtsZ amino acid residues involved in interactions**
PEP40 18	**His33** (1), **Gly34** (1), Arg191, **Gln192** (1), Gln195, Gly196, Ser198, Asp199, Ala202, Val203, Ile228, Val297, **Ile298** (1), **Asn299** (1), Glu301, Leu302, Val307, and Thr309
PEP44 15	**His33** (1), **Gly34** (1), Arg191, Gly192, Gln195, Gly196, Asp199, Ala202, Val203, Ile228, **Asn299** (1), Glu301, Leu302, Val307, Thr309
PEP56 16	His33, **Gly34** (2), **Arg191** (1), Gln192, Gln195, Gly196, Asp199, Val203, **Glu206** (1), Ile228, Thr265, Val297, **Ile298** (1), **Asn299** (1), Glu301, Thr309
PEP58 18	His33, **Gly34** (2), Met35, Arg191, Gln192, **Gln195** (2), Gly196, **Asp199** (1), Ala202, Val203, **Glu206** (1), Ile228, Thr265, Val297, **Ile298** (1), **Asn299** (1), Glu301, and Leu302.

*Residues highlighted in blue: common residues that are involved in contact with all four peptides.

*Underlined Residues: residues in common with PC190723 binding profile

However, as for the static nature of molecular docking studies, these rigid techniques sometimes fail to fully uncover the complex behavior of peptide binding to protein. Therefore, 150 ns

molecular dynamics (MD) simulations are supplemented to further assessment the binding nature of the peptides, and investigate the strength of their complexes with target. In this line, the MD simulations results are discussed in the following sections. It is postulated that the inhibitory potential can be assessed by investigating the stability of complex between the inhibitor and target [43]. A more stable inhibitor–target complex generally indicates a greater likelihood of effective inhibition [43]. RMSD (root mean square deviation) is a typical approach for the assessment of conformational stability of ligand-protein complex during the MD simulations [43]. This analysis measures the displacements of atomic coordinates from the initial point to the final frame. Higher RMSD values or oscillations in the plot reflect possible conformational changes, proposing alterations in structural stability of the complex [43]. Generally, it is observed that almost all of the complexes have gained their equilibrium states almost over the first 20 ns of the simulation period with the highest fluctuations of almost <1.5 Å, except for few slightly drifts which will be discussed (**Fig. 5**). This observation suggests that peptide binding has not introduced any severe conformational alterations in the building block of the target. As for the free protein, the RMSD plot does not go through marked changes over the simulation era, and it is equilibrated with the lowest RMSD average (0.88 Å) (**Fig. 5A**). The apo-protein finds its stable conformation over this period, so this simulation time is likely to be enough for the system.

Among the complexes containing peptides, PEP40 induces larger displacements in the protein structure since its average RMSD is the highest among all (1.46 Å), although the highest RMSD fluctuations stay below 1.5 Å over the simulation (**Fig. 5A**).This result delineates that PEP40-target complex remain stable over the simulation time without any harsh structural changes, while this peptide induces higher conformational flexibility in the target protein compared to the other peptides. However, the complex comprising PEP56 demonstrates an RMSD average of 0.90 Å, which is very close to that of the free FtsZ, with minimal fluctuations between 2.2 Å and 2.5 Å (**Fig. 5A**). This means that this peptide makes a stable complex with the protein, and efficiently, holds the native structure of the target.

As for the complexes containing PEP58 and PEP44, these two peptides have shown moderate average RMSD magnitudes of 0.99 and 1.13 Å, correspondingly (**Fig. 5A**). PEP58's RMSD plot stays

at the same level for the initial half of the simulation time before moderate rise and fluctuations from 3.2 Å to 3.4 Å. Comparatively, the RMSD plot for the complex with PEP44 experiences marginal fluctuations between 2.7 Å and 3.3 Å during the simulation time (**Fig. 5A**). It is noteworthy mentioning that none of the peptides reveal either the RMSD fluctuations above 1.5 Å or continuous conformational drifts, suggesting that target-peptide complexes remain structurally stable throughout the course of simulation. In total, the RMSD findings propose that the FtsZ structure remains stable upon peptide binding, with conformational stability upon the order Free ≈ PEP56 > PEP58 > PEP44 > PEP40, where PEP56 shows the closest structural resemblance to the target, whereas PEP40 binding leads to the highest, yet still stable, flexibility into the FtsZ structure.

The Rg (radius of gyration) and SASA (solvent accessible surface area) are two significant analysis representing vital structural points of view on structural nature and stability of a protein upon ligand binding. The Rg results dedicate that the enzyme structure maintain a highly compact in apo- and peptide-bound states over the course of simulation. It should be noted that the average Rg values for all systems almost fluctuates within a narrow range (19.96 Å and 19.75 Å; nearly 0.2 Å), along with no severe alterations or long-term drift, suggesting that none of the peptides translated any conformational opening or important expansion of the target (**Fig. 5B**). The mean Rg magnitudes for apo-protein, and the systems comprising PEP40, PEP44, PEP56, and PEP58 are 19.84 Å, 19.96 Å, 19.75 Å, 19.81 Å, and 19.79 Å, respectively (**Fig. 5B**). The differences among the complexes (~0.2 Å) means that the overall compactness of protein does not alter remarkably. PEP40 is seen to cause the greatest Rg mean value (19.96 Å), while the increase was negligible (0.12 Å) compared to the free protein. This shows that protein compactness marginally increases upon binding to this peptide, which cooperates to its highest RMSD average value. However, the highest decline in the average Rg magnitudes of the target is seen in complex with PEP44, following by PEP58, and PEP56. This highlights that the protein structure experiences the highest compression after binding to PEP44, and few decreases in the Rg values upon binding to PEP58 and PEP56 shows slightly compactness of the protein structure, supporting the preservation of the native structure of the protein (**Fig. 5B**). These findings reveal the stability of the complexes, which remained structurally compact and well equilibrated over the simulation. The Rg results

corroborate with the RMSD findings, confirming that peptide binding does not compromise the structural integrity of FtsZ. Although PEP40 induced slightly greater structural flexibility according to the RMSD analysis, this did not translate into significant changes in overall protein compactness, whereas PEP44, PEP56, and PEP58 maintained a compact conformation that was comparable to or slightly more compact than the free protein.

The SASA analysis is also investigated, which the SASA values of the protein do not experience severe alterations upon binding to the studied peptides, demonstrating that the peptide binding has not made the protein surface to be extensively exposure by the solvent. Our results show an average SASA value of 137.72 nm^2 for the apo-protein, while this number marginally rises upon binding to the peptides, e.g. the mean SASA magnitudes for the systems comprising PEP40 is the highest among all (143.47 nm^2), followed by PEP56 (139.58 nm^2), PEP44 (138.79 nm^2), and PEP58 (137.86 nm^2). The relatively larger SASA for the PEP40 complex indicates a slight increase in solvent-exposed surface area, which is in line with its higher RMSD and Rg values. However, PEP58 illustrates a mean SASA value very close to that of the free protein, suggesting that this peptides induces limited changes in solvent accessibility while maintaining a favorable and accommodated binding mode. Likewise, PEP44 and PEP56 have exhibited only marginal soars in SASA values. These minimal increases in SASA magnitudes are probably caused by localized adjustments at the peptide-binding interface rather than global conformational changes. These findings are in agreement with the RMSD and Rg results, further demonstrating that peptide binding is accommodated through subtle local rearrangements while preserving the overall structural integrity of FtsZ.

To shed light on each residue oscillations of the protein upon peptide binding, the root mean square fluctuation (RMSF) analysis should be taken into account. Bearing the fundamental role of the PC190723-binding interdomain cleft in mind, which incorporates residues such as Gly196, Asp199, Val203, Val207, Asn208, Leu209, Met226, Asn263, Val297, Thr309, and Ile311 [37], and its proximity to the T7 loop involved in GTP hydrolysis in mind, the RMSF profiles provide more interesting mechanistic insight. As can be seen in Fig 6 A, the RMSF numbers show some increases upon binding to PEP40, with rise in flexibility around the interdomain cleft/T7-loop region, this cooperates with its RMSD results since this peptides induces the largest

conformational flexibility in the protein structure, which this conformational flexibility is translated to each atomic coordinate displacements. These increases might be significant off the residue numbers between 190 and 210.

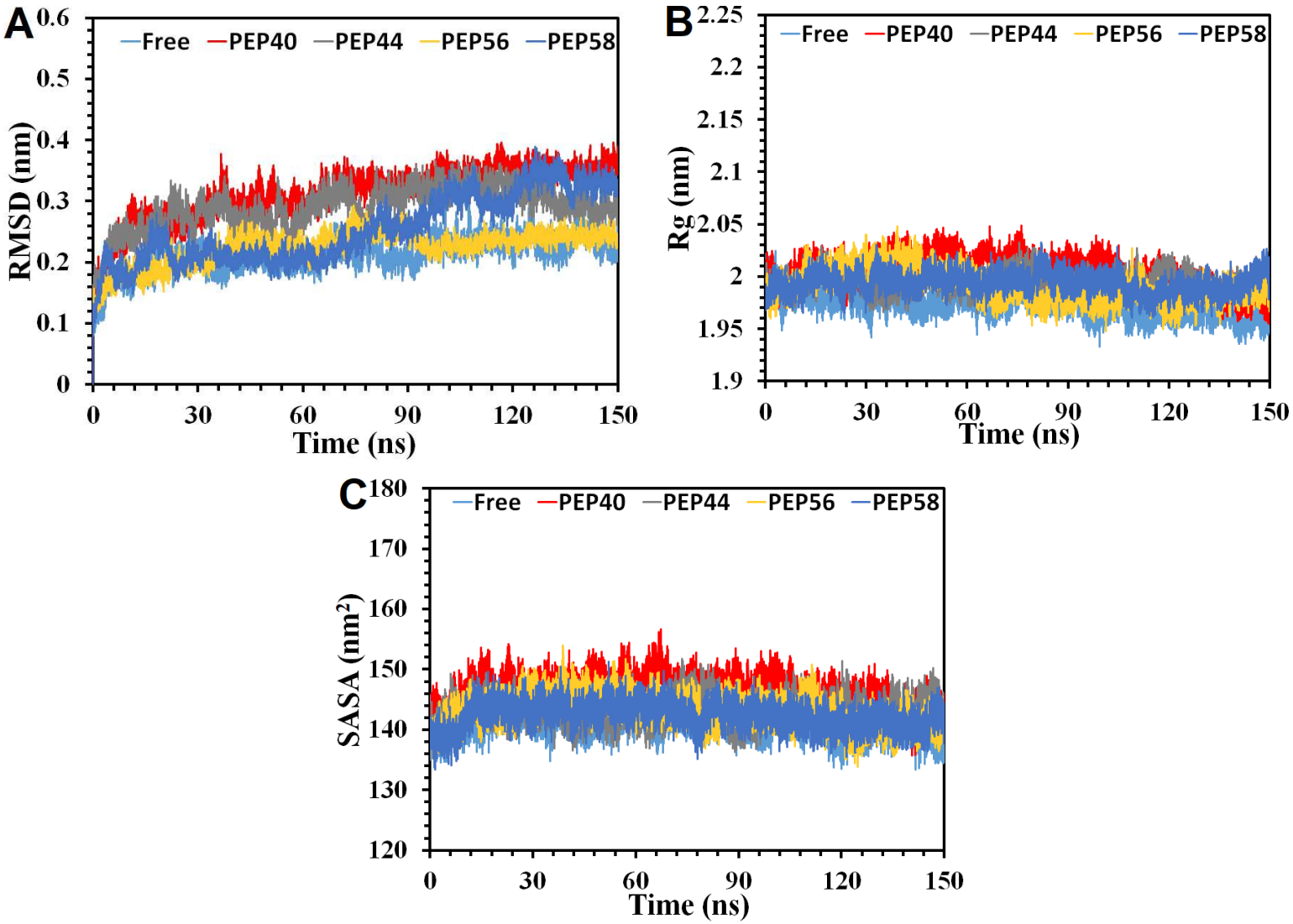


Figure 5. The A) RMSD, B) Rg, and C) SASA profiles of apo-FtsZ (light blue) and in complex with PEP40 (red), PEP44 (gray), PEP56 (light orange), and PEP58 (dark blue).

The RMSF numbers, however, demonstrate lower magnitudes of rising fluctuations after binding to the other three peptides, which lower mobility of each residues can be seen in the order of PEP44 > PEP56 > PEP58. Compared to PEP40, lower flexibility of the target residues upon binding to these three peptides shows their lower movement and mobility. However, the RMSF

fluctuations in the interdomain cleft, especially around residues from 196-210, are predicted to substantially rise upon binding to PEP44, while this region's RMSF oscillations stay either close to that of the free movement or shows lower mobility after binding to PEP56 and PEP58. Also, the RMSF numbers around the other few residues, Met226, Asn263, Val297, Thr309, and Ile311, situated at the interdomain cleft maintain unchanged or showed lower flexibility. The vital key residues for catalytic functions FtsZ includes GTP-binding region-Asp46, Gly104–Gly108, and Glu139; and catalytic hydrolysis region: Asn208, Asp210, Asp213 (T7 loop). Interestingly, except for PEP40, the RMSF magnitudes of the residues located at the catalytic sites in the complexes comprising PEP44, PEP58, and PEP56 are anticipated to have minimal fluctuations, which indicates that these residues experience lower movement after binding to these peptides.

Armed with these results, few suggestions can be made for the consequences of peptide binding on the FtsZ structure and dynamics: PEP40 seems to perturb FtsZ by enhanced local flexibility, whereas PEP44 may induce a more localized alteration of interdomain-cleft dynamics. However, PEP56 and particularly PEP58 appear to maintain or reduce the mobility of key residues within this region, potentially stabilizing a distinct conformational state. Since the interdomain cleft is structurally interconnected with the T7 loop, which plays a critical role in GTP hydrolysis, alterations in the dynamics of this region may influence the conformational transitions underlying FtsZ function [37,44]. Therefore, these peptide-induced dynamic changes may interfere with the conformational transitions required for efficient GTP hydrolysis and FtsZ polymerization. Thus, the peptides might induce their effects through distinct allosteric mechanisms, involving either excessive flexibility or stabilization of a nonproductive conformational state.

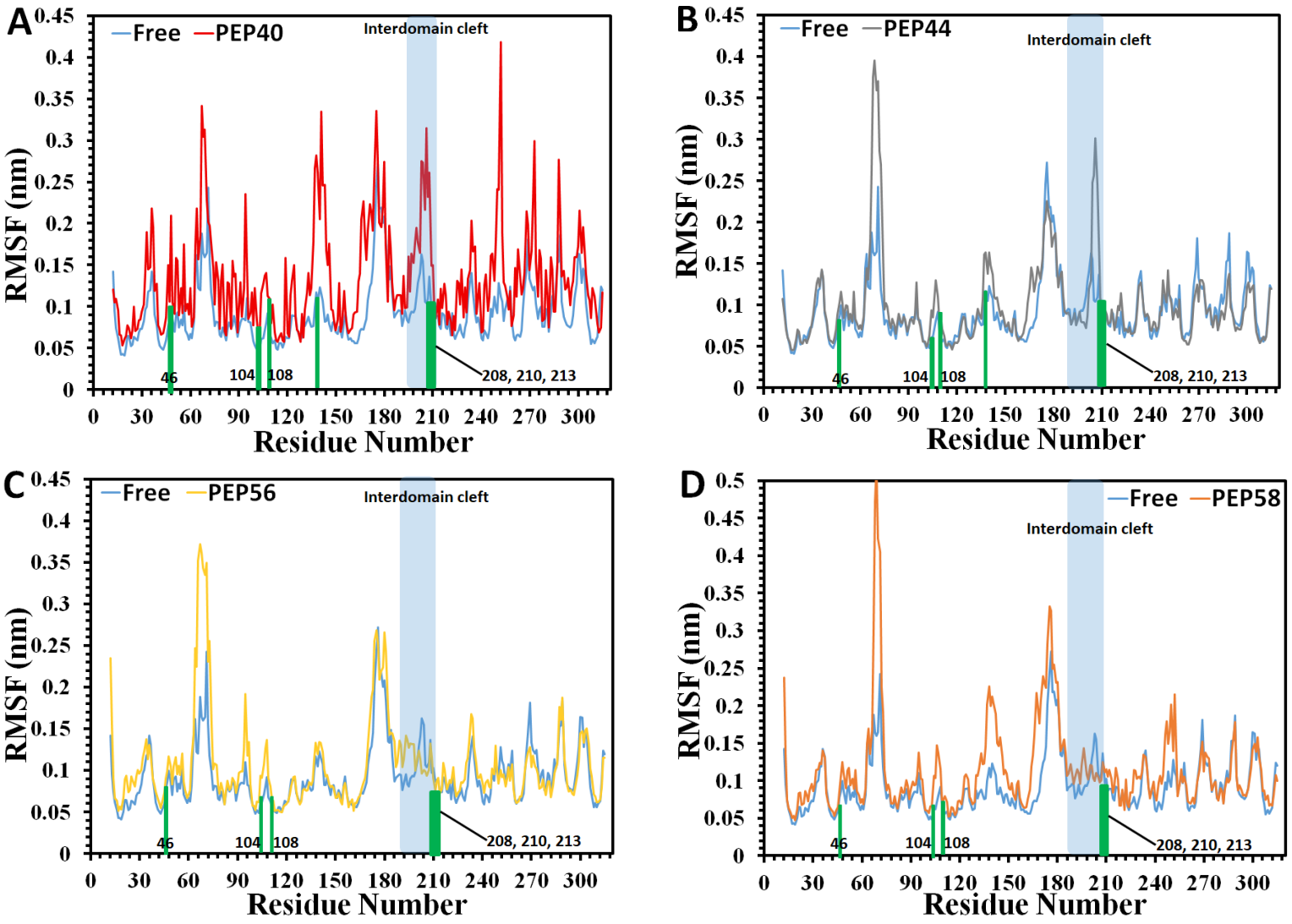
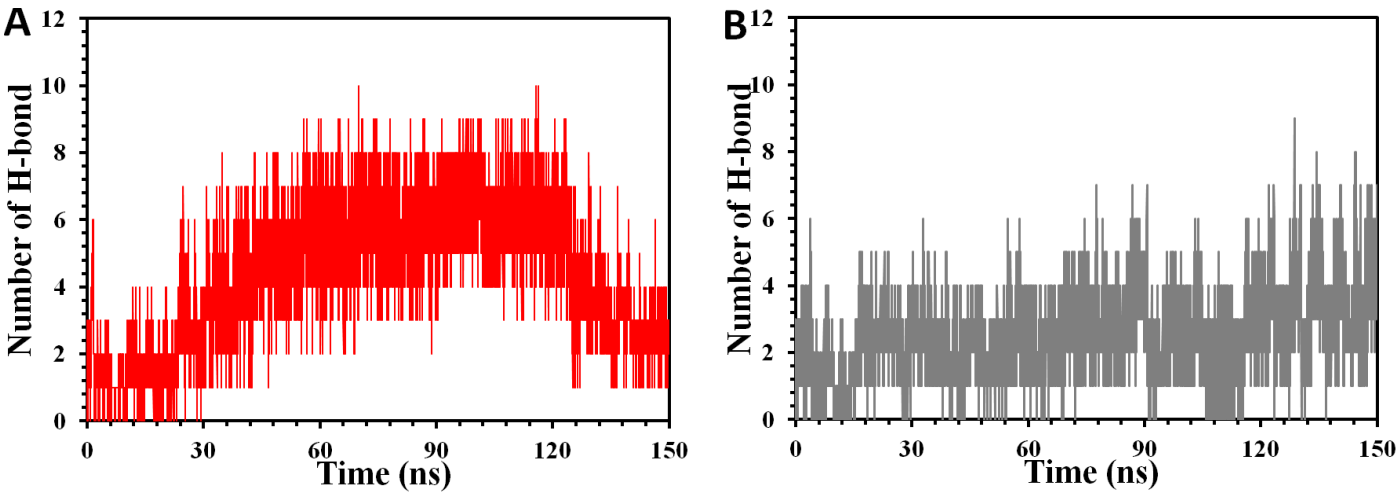


Figure 6. The changes in the RMSF plots of free protein (light blue) and complex with A) PEP40 (red), B) PEP44 (gray), C) PEP56 (light orange), and D) PEP58 (dark blue).

Since hydrogen bonds are of high significance in the stabilization of ligand-protein complexes, we have further investigated hydrogen-bond analysis of the complexes. This represents key perspective on H-bond formation between the peptides and protein in the dynamic nature of MD simulations, which can be compared to static environment of molecular docking. Molecular docking results revealed the formations of 8, 6, 5, and 3 H-bonds for PEP58, PEP56, PEP44, and PEP40 with FtsZ, respectively, suggesting that PEP58 initially established the most extensive polar interaction network, whereas PEP44 formed the fewest contacts. The dynamic nature of the MD

simulations make a different pattern, e.g., the mean numbers of hydrogen bonds are observed to be 2.5 for PEP40, and 4.0 for each one of the other three peptides. Therefore, PEP40 shows a remarkable decrease from its docking value, indicating that few of its generated hydrogen bonds are lost after MD simulations. However, PEP44 illustrates an increase in H-bonds formation with the target from 3 H-bonds in docking to roughly 4 H-bonds during MD, proposing an additional polar contact generated after MD simulations. Compared to docking results with predicted 6 polar contacts for PEP56, this peptide is predicted to lose one hydrogen bond after MD simulation, with approximately four stable H-bonds. PEP58 with the largest polar interactions (8) in molecular docking, around 4 hydrogen bonds are predicted to be stable after MD simulations for this peptide. Overall, the MD results suggest that PEP56, PEP58, and PEP44 organize the most persistent polar contacts with the FtsZ. These interesting results highlight nature of molecular docking and MD simulations; static molecular docking nominate a favorable initial binding pose, whereas MD simulations investigates whether these contacts remain stable under dynamic conditions.



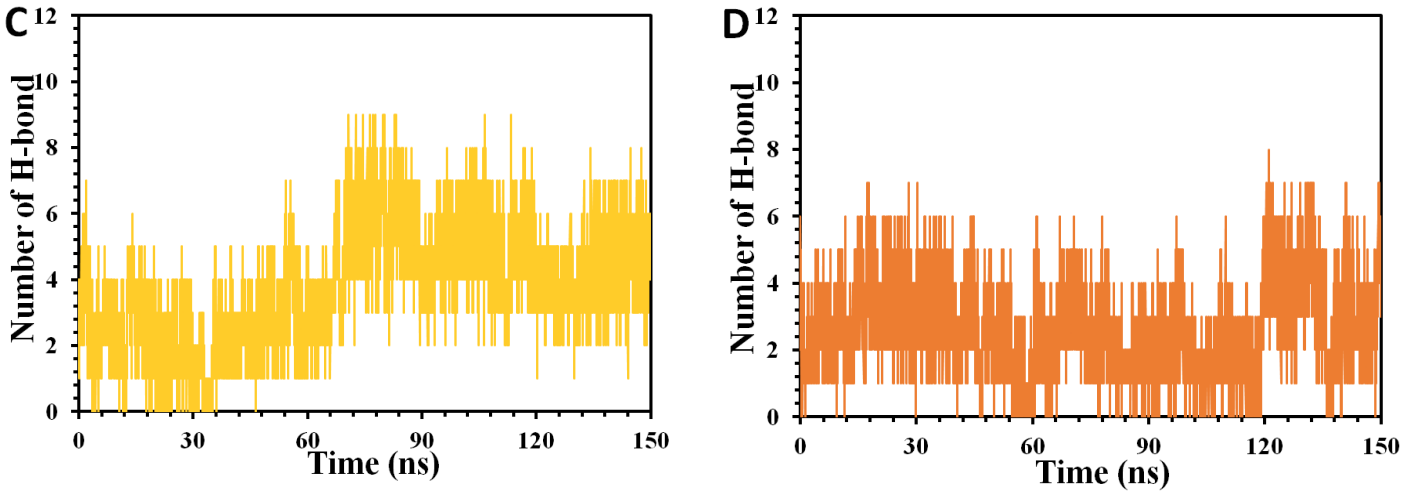


Figure 7. The changes in H-bond versus time between A) PEP40 (red), B) PEP44 (gray), C) PEP56 (light orange), and D) PEP58 (dark blue) with the FtsZ.

Last but not least, structural changes and dynamic characteristics of apo-protein and in complex with the studied peptide are investigated through PCA (principle component analysis). The apo-FtsZ exhibits two distinct and expanded clusters, showing the adopted conformational range of protein over the simulation. Free protein shows the highest mobility range since it expands from -2.5 to 1.8 on PC1 (range = 4.3) and form -1.2 to 1.0 on PC2 (range = 2.2), proposing that the structure of free FtsZ has a higher freedom to move. However, the PCA plots of the systems comprising the studied peptides face some changes in terms of movement paradigm and reduced mobility range on the initial two PCs. Besides, all of the peptides, except for PEP40, caused some decreases in the mobility ranges of protein either on PC1 or on PC2. As it was observed in the RMSD, Rg, and SASA plots, PEP40 had the highest averages, so its PCA plot, compared to that of the free protein, is predicted to increase on PC2; expanding between -1.3 and 1.3 (range 2.6); and maintain the same on PC1 from -2 to 2.1 (range = 4.1). This cooperates with the Rg, and SASA findings, suggesting that protein experiences a slightly higher flexibility, and freedom to move upon binding to PEP40 with no sign of unfolding phenomenon. However, the other three PCA plots reveal more compressed and clustered compare to that of the target, these results are in line with those of Rg and SASA findings for PEP44, PEP56, and PEP58. These observations suggest that structural conformation of the FtsZ is predicted to become more clustered and compressed upon binding to these there ligands. For example, the PCA diagram of protein in

complex with PEP44 is clustered on the first two PCs; from -1.4 to 1.3 on PC1 (range = 2.7) and from -1.3 to 1.3 on PC2 (range = 2.6). Protein mobility pattern becomes slightly more compressed upon binding to PEP56, which extends between -1.2 and 1.1 on (range = 2.3) and from 1.16 to 0.92 (range =2.08) on the first two axis. PEP58 also produces a narrower PC distribution since the protein mobility variates from -1.5 to 1.6 on PC1 (range = 3.1) and between -1.0 and 0.9 on PC2 (range = 1.9). As for any possible change in the protein movement pattern, it seems that the protein mobility paradigm somehow changes upon binding to all of the peptides, while the most severe deformity can be seen upon binding to the order of PEP44 > PEP56 > PEP58 > PEP40.

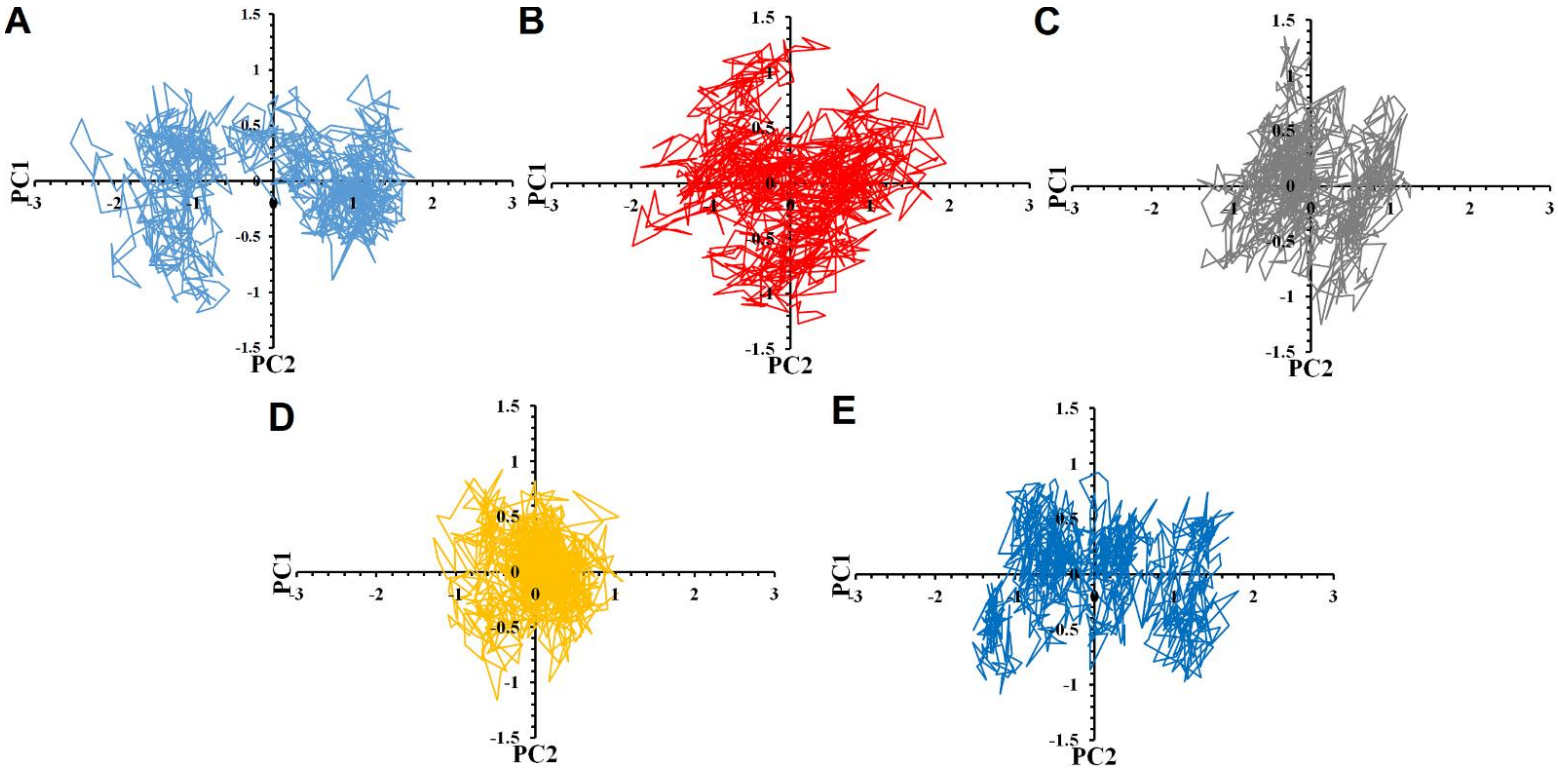


Figure 8. The alterations in the PCA plots of A) free FtsZ and in complex with B) PEP40 (red), C) PEP44 (gray), D) PEP56 (light orange), and E) PEP58 (dark blue).

In this study, although the entropic analysis of the complexes has been assessed through RMSF and PCA, the enthalpic aspects should be considered as well by computing the total binding energies of each protein-peptide complex using MM/PBSA approach (**Table 4**). The enthalpic share of the complexes has revealed interesting results since the molecular docking showed the strongest binding energies follow the order of PEP58 > PEP44 > PEP56 > PEP40 (–73.0) kcal/mol,

while the calculated total binding energies by MM/PBSA indicates a little different pattern with those of the HADDOCK scores, which the strongest complexes are made with the target by the order of PEP44 (–243.13) > PEP58 (–230.10) > PEP40 (–193.03) > PEP56 (–143.79) kJ/mol. This intriguing result comes from the dynamic nature of MD simulations, highlighting the eminent role of solvation and entropic contributions in MD simulations, while it is absent in rigid environment of molecular docking. According to the MM/PBSA results, PEP44 establishes the strongest complex with the target protein, which is predominantly governed by its electrostatic energy (–269.85 kJ/mol), the highest share among all peptides. This cooperates with its docking profile since most of its contacts with the target are nonpolar interactions, while it has shown a moderate van der Waals (VdW) term (–98.07 kJ/mol). However, its total binding energy suffers from a high polar solvation penalty (+139.25) partially offsets electrostatics, yet the net remains superior. According to its building block, PEP44 (I65F/A69F/E70V) incorporates two phenylalanines that improve π-stacking with aromatic residues in the interdomain cleft, while valine at position 70 reduces desolvation cost, consistent with its low SASA penalty (–13.46). Compared to this, PEP58 (I65H/A69M/E70L) possesses the strongest VdW contribution (–239.97 kJ/mol)–approximately 2.5 times greater than PEP44–demonstrating an optimized hydrophobic packing from methionine and leucine substitutions. These findings also match the docking results since PEP58's docking profile showed the highest number of non-polar interactions with the target. Nonetheless, its weaker electrostatic share (–122.61 kJ/mol) and higher polar solvation (+148.26 kJ/mol) have negative effects on its total binding energy compared to PEP44. However, interestingly, although PEP58 formed the highest number of H-bonds in docking (8) and the greatest contact network in docking, MD analysis showed only ~4 persistent H-bonds, suggesting that some polar contacts are transient and contribute less enthalpically than anticipated.

It should be noted that PEP56 and PEP40 both possess the E70I substitution, which seems it has a deficient role on the total binding energies since these two peptides illustrate weaker total energies compared to the other two peptides. PEP56 is predicted to establish the weakest complex with the target due its lower binding energy (-143.79 kJ/mol), which composed of a moderate vdW share (–74.84 kJ/mol) and the lowest electrostatic share (–136.95 kJ/mol). Its high polar solvation penalty (+81.52 kJ/mol) also reduces its total binding energy, suggesting that

introducing one methionine at position at position 69 without a corresponding aromatic partner fails to establish a cohesive interaction network. Compared to this, PEP40 has formed a stronger binding energy (–193.03 kJ/mol), yet lower than those of PEP44 and PEP58. Interestingly, its higher SASA contribution (–12.36 kJ/mol) highlights greater solvent exposure, which cooperates with its escalated RMSD and Rg average magnitudes, suggesting some conformational loosening.

To make comparison between molecular docking and MM/PBSA results, it is interesting to stress that interaction counts and shape complementary are prioritized in molecular docking, but MM/PBSA approach take significant effects of solvents and energetic quality. The greater share of electrostatic contacts of PEP44 may be related to its capability to make polar contacts with polar residues (e.g., His33, Gly34, Asn299), as reflected by its stable 4 H-bonds after MD simulations. The superiority of PEP58 in making VdW contacts may arise from extensive hydrophobic contacts (e.g., with Val203, Val297, Leu302) that mimic binding profile of PC190723, yet its polar solvation penalty decreases net gain. These two peptides translated marginal conformational perturbation (RMSD <1.2 Å, compact Rg ~19.8 Å) and maintained the native dynamics of FtsZ's, as proposed by PCA with clustered conformations. Taken all together, PEP44 and PEP58 seem to be the most promising candidates. PEP44 shows the best overall thermodynamic stability, governed by strong electrostatic anchoring, while PEP58 provides superior hydrophobic complementarity and a broader interaction interface. The complementary binding mechanisms may propose that these peptides are likely to act as promising allosteric inhibitors of FtsZ, potentially hindering polymerization by distinct pathways. Further experiments such as bacterial growth inhibition and GTPase activity tests should be supplemented to validate their inhibitory effects.

Table 4. The calculated MM/PBSA interaction energies for the chosen peptides in complex with FtsZ (kJ/mol).

Peptide No.	VdW	Elec	Polar solvation	SASA	Total
PEP40	-69.117	-208.785	+93.025	-12.36	-193.025
PEP44	-98.07	-269.85	+139.25	-13.46	**-243.13**
PEP56	-74.84	-136.95	+81.52	-13.52	-143.79

PEP58	-239.97	-122.605	+148.26	-15.78	**-230.095**

Discussion

Computer-based methods are of high importance in drug design and developments, facilitating investigation of potential ligand–target interactions before experimental assessment. By integrating computational screening with structural and energetic analyses, recent investigations paved the way for the identification of promising compounds capable of interacting with and potentially inhibiting FtsZ [45,46]. Bearing the promising antibacterial potential of the bovine milk Lactoferrin in mind [15], our group are motivated to set a computational workflow to design novel lacroferrin-derived peptides for identification of new peptide-based inhibitors targeting the interdomain cleft of Staphylococcus aureus FtsZ. Our computational method incorporates protein–protein docking, identification of residue prone to mutation by MM/PBSA decomposition, systematic mutation, peptide library generation, toxicity/allergenicity filtering, molecular docking, and MD simulations. Our molecular docking studies reveal four candidates, PEP40, PEP44, PEP56, and PEP58, with PEP58 showing the most favorable score (−75.2) and PEP44 ranking second (−74.6), showing potentially stronger HADDOCK sores than that of the peptide template. It is also observed the introduction of I65, A69, and E70 as mutation-sensitive spots leads to a rational basis for sequence optimization rather than relying exclusively on empirical peptide screening. This provides a key strength of our study and extends previous computational FtsZ-peptide studies. Pieraccini and coworkers designed FtsZ-targeting oligopeptides using MD simulations that subsequently demonstrated functional activity in vitro, establishing the feasibility of computationally guided peptide development [47]. Similarly, Di Somma et al. modified Temporin-L and showed that optimized analogues established stable FtsZ complexes and inhibited both FtsZ enzymatic and polymerization activities [48]. In another job, Liu and his team combined virtual peptide screening, docking, MD, and experimental antibacterial evaluation against FtsZ, identifying five peptides that inhibited bacterial growth without directly suppressing FtsZ GTPase activity [49].

In comparison to the previous researches, the present study may possess few distinctive advantages. To the best of our knowledge, no peptide-derived inhibitors based on bovine milk

Lactoferrin have previously been developed against FtsZ. Besides, the peptides are derived from a naturally occurring milk-protein sequence and subsequently optimized through residue-level energetic analysis, providing a biologically inspired starting point for peptide discovery. Rationally residue substitution at positions 65, 69, and 70 of the peptide template remarkably improved the binding affinity. Due to static nature of molecular docking that seeks the best binding pose in a static nature, we have also assessed the complex strength of the peptides with the target protein in a more dynamic environment to mimic the physiological environment. In this line, the strength of the complexes are investigated not only in terms of enthalpic points of view (RMSF and PCA), but also in enthropic aspects are taken into account. This feature represents multidimensional assessment of peptide-induced structural and dynamical changes, which distinguishes our job with the last works. Our simulations results illustrate that the FtsZ structure does not experience a global destabilization upon peptide binding. Although PEP40 increased the average RMSD, Rg, and SASA mean values of the target, indicating introducing localized conformational adjustments in the FtsZ PC binding site after binding to this peptide. Thermodynamic stability of the complexes are comprehended using Rg and SASA results; among the peptide, PEP58 and PEP44 made the target conformation become more compact, while PEP56 translated minimal changes in protein structure, which caused the protein conformation to experience the highest compactness, as observed by PCA analysis. PEP58 was additionally characterized by the largest docking interaction network and the highest initial hydrogen-bond count, while approximately four hydrogen bonds persisted during MD, indicating that several favorable polar contacts survived structural relaxation. After fully consideration of the entropic analysis of the complexes by RMSF and PCA, the enthalpic aspects are taken into account by the total binding energy calculation using MM/PBSA technique (**Table 4**). Among the chosen peptides, the peptide in the order of PEP56 > PEP58 > PEP44 formed the strongest complexes with the target protein, which was confirmed by enthropic assessment through total binding free energy by MM/PBSA calculations. MM/PBSA results delineated that the strongest complexes are established by order of PEP44 > PEP58 > PEP40 > PEP56. Besides PEP44 shows the best overall thermodynamic stability, governed by electrostatic anchoring, with stable H-bonds and low SASA penalty. PEP58 provides superior hydrophobic complementarity and a broader binding interface, yet suffers from higher solvation.

Both maintain native dynamics of FtsZ with marginal perturbation. Their complementary mechanisms suggest promising allosteric inhibition of FtsZ via distinct pathways.

However, although our computational workflow provides significant aspects toward identification of novel peptide-based inhibitors against FtsZ, few limitations in our method must be acknowledged. Initially, molecular docking study of peptide to FtsZ by HADDOCK online server incorporates experimental or predicted interface information through active and passive residues, improving the biological relevance of predicted binding poses, while this online webserver may suffer from a couple of obstacles, e.g., this platform might take local flexibility into account, while large-scale structural alterations in the protein conformation upon peptide binding are not fully captured. Thus, to tackle this obstacle, we have assessed the dynamic nature of the FtsZ in apo state and in complex with the peptides to comprehend the effects of the peptides on the conformation and dynamics of the target. By doing this, the stability of the protein-peptide complexes can be investigated in a more dynamic environment, somehow in a more biological-relevant nature. Despite the higher flexibility is provided by MD simulations, however, these computational approaches themselves bear some demerits such as the computational time required for adequate sampling and the accuracy of the employed force fields, which should be taken into consideration. Although our computational work provides significant data on designed peptides modulatory/inhibitory activities against FtsZ, future experimental tests, including GTPase activity and bacterial growth inhibition assessments, are suggested to confirm their inhibitory effects. To sum, our extensive computational findings propose PEP44 and PEP58 and the most promising lead candidates against FtsZ for experimental validation and subsequent preclinical development.

Conclusion

The rapid escalation of antibiotic resistance highlights the pressing need to find and develop new antibacterial agents. FtsZ, a bacterial cell-division protein central to Z-ring formation during cytokinesis, emerges as a validated but still underutilized target—particularly through its allosteric interdomain cleft, the same site engaged by the inhibitor PC190723. Here, bovine milk lactoferrin, a pharmaceutical protein already known for its antibacterial activity, was employed

for the first time as a scaffold to design novel peptides against FtsZ. Molecular docking of the template against the FtsZ PC-binding pocket led to a 10-residue peptide template, which was subsequently optimized via MM/PBSA-guided mutations at three key hotspot residues (65, 69, and 70), generating a peptide library that was then filtered for safety and binding performance. Two candidates, PEP44 and PEP58, indicated the best docking scores and the most favorable MM/PBSA binding energies; each stabilized through distinct but complementary electrostatic and hydrophobic interactions. MD simulations further verified that both peptides maintain FtsZ's native structural behavior while reinforcing the interdomain cleft, mirroring the allosteric mechanism of PC190723. Taken all together, this work establishes a pioneering lactoferrin-based peptide design strategy targeting FtsZ, with PEP44 and PEP58 standing out as strong candidates for future experimental testing and development as next-generation antibacterial therapeutics.

Declaration of competing interest

The authors declare that there is no financial or personal relationships that could influence the paper.

Funding Declaration

No funding is available for this research.

Data availability

Upon a reasonable request, the data supporting the results of this article will be made available by the corresponding responsible author.

Author Contributions Statement

M.H. H. performed molecular docking, MM/PBSA calculations, and MD simulations, analyzed the data, and drafted the manuscript. **V. A.** supervised the project, designed the study, toxicity/allergenicity predictions, contributed to methodology development, and revised the manuscript critically for important intellectual content. **A. Z.** contributed to peptide library screening, data curation, and visualization of structural data, and assisted with validation of computational protocols. All authors read and approved the final manuscript.

References

1 Ahmad, M., Aduru, S. V., Smith, R. P., Zhao, Z. & Lopatkin, A. J. The role of bacterial metabolism in antimicrobial resistance. *Nature Reviews Microbiology* **23**, 439-454, doi:https://doi.org/10.1038/s41579-025-01155-0 (2025).

2 Süssmuth, R. D., Kulike-Koczula, M., Gao, P. & Kosol, S. Fighting antimicrobial resistance: innovative drugs in antibacterial research. *Angewandte Chemie International Edition* **64**, e202414325 (2025).
3 Hurley, K. A. *et al.* Targeting the bacterial division protein FtsZ. *J. Comput. Chem.* **59**, 6975-6998 (2016).
4 Fujita, J. *et al.* Structural basis for the interaction between the bacterial cell division proteins FtsZ and ZapA. *Nature Communications* **16**, 5985, doi:10.1038/s41467-025-60940-w (2025).
5 Lock, R. L. & Harry, E. J. FtsZ as an Antibacterial Target: Status and Guidelines for Progressing This Avenue. *Biochimica et Biophysica Acta* **1784**, 12-19, doi:10.1016/j.bbapap.2007.09.018 (2008).
6 Radha Mahendran, F., Palanimuthu, M. & Subasri, S. Sequence and structural analysis of FtsZ homologs and comparison of bacterial FTsZ with eukaryotic tubulins. *Indian Journal of Science and Technology* **4** (2011).
7 Nußbaum, P. *et al.* Proteins containing photosynthetic reaction centre domains modulate FtsZ-based archaeal cell division. *Nature Microbiology* **9**, 698-711, doi:10.1038/s41564-024-01600-5 (2024).
8 Vemula, D., Maddi, D. R. & Bhandari, V. Homology modeling, virtual screening, molecular docking, and dynamics studies for discovering Staphylococcus epidermidis FtsZ inhibitors. *Frontiers in Molecular Biosciences* **Volume 10 - 2023**, doi:10.3389/fmolb.2023.1087676 (2023).
9 Domadia, P. N., Bhunia, A., Sivaraman, J., Swarup, S. & Dasgupta, D. Berberine targets assembly of Escherichia coli cell division protein FtsZ. *Biochemistry* **47**, 3225-3234 (2008).
10 Beuria, T. K., Santra, M. K. & Panda, D. Sanguinarine blocks cytokinesis in bacteria by inhibiting FtsZ assembly and bundling. *Biochemistry* **44**, 16584-16593 (2005).
11 Haydon, D. J. *et al.* An inhibitor of FtsZ with potent and selective anti-staphylococcal activity. *Science* **321**, 1673-1675 (2008).
12 Zhang, Q. Antimicrobial peptides: from discovery to developmental applications. *Applied and Environmental Microbiology* **91**, e02115-02124 (2025).
13 Islam, T., Tamanna, N. T. & Sagor, M. S. Antimicrobial Peptides: A Promising Solution to the Rising Threat of Antibiotic Resistance. **16**, doi:10.3390/pharmaceutics16121542 (2024).
14 Chi, J. *et al.* Combating the post-antibiotic era crisis: antimicrobial peptide/peptidomimetic-integrated combination therapies and delivery systems. *Journal of Materials Chemistry B* **13**, 11996-12019, doi:10.1039/d5tb01424g (2025).
15 Xu, Y., Wang, Y., He, J. & Zhu, W. Antibacterial properties of lactoferrin: A bibliometric analysis from 2000 to early 2022. *Frontiers in Microbiology* **Volume 13 - 2022**, doi:10.3389/fmicb.2022.947102 (2022).
16 Meleti, E., Koureas, M., Manouras, A., Giannouli, P. & Malissiova, E. Bioactive Peptides from Dairy Products: A Systematic Review of Advances, Mechanisms, Benefits, and Functional Potential. *Dairy* **6**, 65 (2025).
17 Dhar, H. *et al.* Functional attributes of bioactive peptides of bovine milk origin and application of in silico approaches for peptide prediction and functional annotations. *Critical reviews in food science and nutrition* **64**, 9432-9454 (2024).
18 Wang, Z., Xu, J. & Zeng, X. Recent Advances on Antimicrobial Peptides from Milk: Molecular Properties, Mechanisms, and Applications. **72**, 80-93, doi:10.1021/acs.jafc.3c07217 (2024).
19 Morrin, S. T., Buck, R. H., Farrow, M. & Hickey, R. M. Milk-derived anti-infectives and their potential to combat bacterial and viral infection. *Journal of Functional Foods* **81**, 104442, doi:https://doi.org/10.1016/j.jff.2021.104442 (2021).
20 Khatoon, A., Khan, U. M. & Kaur, M. Exploring the antimicrobial potentials and thermal stability of bovine lactoferrin against foodborne pathogens. *International Journal of Food Science and Technology* **60**, vvae019 (2025).

21 Bielecka, M., Cichosz, G. & Czeczot, H. Antioxidant, antimicrobial and anticarcinogenic activities of bovine milk proteins and their hydrolysates - A review. *International Dairy Journal* **127**, 105208, doi:https://doi.org/10.1016/j.idairyj.2021.105208 (2022).
22 Kowalczyk, P. *et al.* The Lactoferrin Phenomenon—A Miracle Molecule. *Molecules* **27**, 2941 (2022).
23 Jiang, R., Liu, L., Du, X. & Lönnerdal, B. Evaluation of bioactivities of the bovine milk lactoferrin–osteopontin complex in infant formulas. *Journal of Agricultural and Food Chemistry* **68**, 6104-6111 (2020).
24 Jin, L. *et al.* Improving expression of bovine lactoferrin N-lobe by promoter optimization and codon engineering in Bacillus subtilis and its antibacterial activity. *Journal of agricultural and food chemistry* **67**, 9749-9756 (2019).
25 Avery, T. M. *et al.* Analysis of antimicrobial and antibiofilm activity of human milk lactoferrin compared to bovine lactoferrin against multidrug resistant and susceptible Acinetobacter baumannii clinical isolates. *ACS infectious diseases* **7**, 2116-2126 (2021).
26 Hong, R. *et al.* A review of the biological activities of lactoferrin: Mechanisms and potential applications. *Food & Function* **15**, 8182-8199 (2024).
27 Li, B. *et al.* Interaction between dietary lactoferrin and gut microbiota in host health. *Journal of Agricultural and Food Chemistry* **72**, 7596-7606 (2024).
28 Dyrda-Terniuk, T. & Pomastowski, P. The multifaceted roles of bovine lactoferrin: Molecular structure, isolation methods, analytical characteristics, and biological properties. *Journal of Agricultural and Food Chemistry* **71**, 20500-20531 (2023).
29 Hu, C., Shen, W., Xia, Y., Yang, H. & Chen, X. Lactoferrin: Current situation and future prospects. *Food Bioscience* **62**, 105183, doi:https://doi.org/10.1016/j.fbio.2024.105183 (2024).
30 Sohrabi, S. M., Niazi, A., Chahardoli, M., Hortamani, A. & Setoodeh, P. In silico investigation of lactoferrin protein characterizations for the prediction of anti-microbial properties. *Molecular Biology Research Communications* **3**, 85 (2014).
31 Yang, Z. *et al.* Antibacterial mechanism of a novel bovine-derived peptide F1 against colistin-resistant Escherichia coli through ClpP, ClpX and YihG. *LWT* **223**, 117726, doi:https://doi.org/10.1016/j.lwt.2025.117726 (2025).
32 Du, R.-L. *et al.* Discovery of FtsZ inhibitors by virtual screening as antibacterial agents and study of the inhibition mechanism. *RSC Medicinal Chemistry* **13**, 79-89 (2022).
33 Kusuma, K. D., Payne, M., Ung, A. T., Bottomley, A. L. & Harry, E. J. FtsZ as an Antibacterial Target: Status and Guidelines for Progressing This Avenue. *ACS Infectious Diseases* **5**, 1279-1294, doi:10.1021/acsinfecdis.9b00055 (2019).
34 Hirshman, S. P. & Whitson, J. Steepest descent moment method for three-dimensional magnetohydrodynamic equilibria. (Oak Ridge National Lab.(ORNL), Oak Ridge, TN (United States), 1983).
35 Sharma, A. K., Poddar, S. M. & Chakraborty, J. A mechanism of salt bridge-mediated resistance to FtsZ inhibitor PC190723 revealed by a cell-based screen. **34**, ar16, doi:10.1091/mbc.E22-12-0538 (2023).
36 Tan, C. M. *et al.* Restoring methicillin-resistant Staphylococcus aureus susceptibility to β-lactam antibiotics. *Science translational medicine* **4**, 126ra135-126ra135 (2012).
37 Pradhan, P., Margolin, W. & Beuria, T. K. Targeting the Achilles Heel of FtsZ: The Interdomain Cleft. *Frontiers in Microbiology* **Volume 12 - 2021**, doi:10.3389/fmicb.2021.732796 (2021).
38 Moghaddam, N., Ramazani, A. & Zarei, A. Rational design of k-casein peptides to modulate GSK-3B dynamics for Alzheimer's therapy. *Scientific Reports* **16**, 12768, doi:10.1038/s41598-026-42103-z (2026).

39 Vangone, A. & Bonvin, A. M. J. J. Contacts-based prediction of binding affinity in protein–protein complexes. *eLife* **4**, e07454, doi:10.7554/eLife.07454 (2015).
40 Kuntz, I., Chen, K., Sharp, K. & Kollman, P. The maximal affinity of ligands. *Proceedings of the National Academy of Sciences* **96**, 9997-10002 (1999).
41 Branden, C. I. & Tooze, J. *Introduction to protein structure*. (Garland Science, 2012).
42 Andreu, J. M. *et al.* The antibacterial cell division inhibitor PC190723 is an FtsZ polymer-stabilizing agent that induces filament assembly and condensation. *The Journal of biological chemistry* **285**, 14239-14246, doi:10.1074/jbc.M109.094722 (2010).
43 Zareei, S., Pourmand, S., Eskandarzadeh, M. & Massahi, S. In silico anti-alzheimer study of phytochemicals from Lamiaceae family through GSK3-β inhibition. *Scientific Reports* **14**, 834, doi:10.1038/s41598-023-47069-w (2024).
44 Artola, M., Ruíz-Avila, L. B. & Ramírez-Aportela, E. The structural assembly switch of cell division protein FtsZ probed with fluorescent allosteric inhibitors. **8**, 1525-1534, doi:10.1039/c6sc03792e (2017).
45 S R, M. *et al.* In-silico screening of marine fungal metabolites identifies potential FtsZ inhibitors against MDR-tuberculosis through docking and molecular dynamics analysis. *Scientific Reports* **16**, 4030, doi:10.1038/s41598-025-34116-x (2026).
46 Kifayat, S. *et al.* An in silico approach for identification of lead compound as FtsZ inhibitor. *Molecular Diversity* **28**, 3937-3948, doi:10.1007/s11030-023-10787-4 (2024).
47 Pieraccini, S. *et al.* Computer aided design of FtsZ targeting oligopeptides(†). *RSC Adv* **3**, 1739-1743, doi:10.1039/c2ra21886k (2013).
48 Di Somma, A., Canè, C. & Moretta, A. Interaction of Temporin-L Analogues with the E. coli FtsZ Protein. **10**, doi:10.3390/antibiotics10060704 (2021).
49 Liangwang, L., Yuwei, Z., Fangfang, R., Yi, M. & Dayong, W. Molecular docking, and molecular dynamic and antibacterial analyses of polypeptide inhibitors targeting FtsZ protein. *热带生物学报 (中英文)* **14**, 269-278 (2023).

Supplementary Files

This is a list of supplementary files associated with this preprint. Click to download.

- SupportingInformation.docx